UNIVERSITY OF CALIFORNIA
SANTA CRUZ

EXPERIMENTAL STUDY OF NATURALISTIC GRANULAR FLOW RHEOLOGY

A dissertation submitted in partial satisfaction
of the requirements for the degree of

DOCTOR OF PHILOSOPHY

in

EARTH SCIENCES

by

Stephanie Taylor

December 2018

The Dissertation of Stephanie Taylor is approved:

Professor Emily Brodsky, chair

Professor Susan Schwartz

Andrew Rathbun, Ph.D.

Lori Kletzer
Vice Provost and Dean of Graduate Studies

Table of Contents

List of Figures

Abstract

Experimental study of naturalistic granular flow rheology

Stephanie Taylor

Granular materials are central to a wide range of earth science processes. The majority of granular flow rheology experiments and theory describes flows composed of smooth spheres, but natural shear flows are composed of particles exhibiting a range of irregular shapes, sizes, and material properties. For natural hazards involving granular media, like landslides and earthquakes, it is important to understand how the complexity of natural grains affects the transition between nearly static slow moving shear flow regimes and dilatational fast moving shear flow regimes. The transition between these end member regimes can take many forms and occur over orders of magnitude of velocity and pressure conditions. Integrating an understanding of the effects of different material properties and grain shape into velocity phase regimes will allow for a complete energy balance to be drawn up for granular shear flow. Such an understanding will result in effective predictions of rheological behavior based on certain material characteristics and boundary conditions and will answer an enduring and fundamental physics question of how energy entering into a granular system is dissipated. I develop a new method for measuring fluctuation energy in granular shear flow experiments with acoustic energy, and I use this method to examine how internally induced vibrations affect the mechanics of transitional regime flows and the dependence of these mechanics on the material properties of the solid grains that

make up the flow. I find that grain shape and material capacity for plastic damage can change how energy is dissipated in a shear flow, which in turn affects the overall rheology of the system.

Acknowledgments

This work was supported by the University of California Eugene Cota-Robles Fellowship, the Army Office of Basic Research under award W911NF-15-1-0012, and the Zhen and Ren Wu Memorial Award Fund in Geophysics. Many thanks for great patience and technical assistance from Dan Sampson of the Department of Earth & Planetary Sciences, and Dave Thayer and Joe Cox of the UCSC Machine Shop; Earl O'Bannon, Cara Vennari and the UCSC Mineral Physics Lab for assisting with and allowing use of the Raman spectrometer; Jeremy Hourigan and Terry Blackburn for allowing use of the Frantz magnetic separator, Shatterbox and sieves; and Colin Phillips and Doug Jerolmack of the University of Pennsylvania Sediment Dynamics Laboratory for assisting with and allowing use of the Retsch Technology Camsizer Particle Analyzer.

I owe a great deal of gratitude to my committee members, Susan Schwartz, Andy Rathbun and especially my primary advisor, Emily Brodsky. Their guidance through the exploratory phases of this ambitious project were indispensable. Emily's assistance and mentorship in particular have helped me dig deeper into and find my footing in this area of research, which has proven to be very rich.

Constructive discussions with Shalev Siman-Tov and Nicholas van der Elst added greatly to the quality of my experiments and analysis, as did the work of undergraduate experimentalists Kristina Okamoto and Marshall Danese. Collaborators Abram Clark, David Henann, Shihong Li and Behrooz Ferdowsi have

contributed many insights from the granular physics and geomorphology communities. Special thanks also to Karen Daniels and Nathalie Vriend for helpful conversations and introductions.

Fellow graduate students and postdoc researchers Claire Masteller, Carolyn Begeman, Megan Avants, Rachel Lauer, Delphine Defforey, Dustin Winslow, Vincent Allègre, Patrick Fulton and Grace Barcheck provided inspiration and support at critical moments throughout the process of completing this work. I also found encouragement and friendship in GEODES, which was a joy to be a part of.

Finally, I am indebted to my family and friends who have helped me in myriad ways over the course of completing this work. My parents, Roy and Kathy Taylor, my partner Ian Garrick-Bethell, and my friend Praxia Apostle acted as sounding boards and cheerleaders, and I could not have completed these projects without them. Friends Jenna Scarpelli, Darby Begeman, Dave Maher, Mary London, Jessica Gutteridge, Brigitte Gordon, Kate Jackson, Julia Pudlin, Morgan Maeder, Tamara Weiss, Courtney Valiga, Ashley Boyd, Cecilia Connor and family Jim Taylor and Patty Coto also all provided crucial support and assistance for which I am very thankful.

Preface

Granular flows are ubiquitous in nature, yet defy easy characterization or simple rheological laws. A box of sand at rest appears to behave like a solid and can easily support the weight of an object resting on top of the sand. The same box of sand, when tilted, will pour out onto the floor like a liquid. Turn a leaf-blower on and the sand will blow everywhere, filling the room and behaving much like colliding molecules of a gas. Establishing a constitutive law that effectively describes all of these behaviors has been a major challenge in the field of granular physics.

Granular materials are central to a wide range of earth science processes. Sands, muds, soils, pebbles, boulders, and ground up rock in fault damage zones are all granular materials. Natural shear flows made up of these types of materials pose particular challenges scientifically, but also tend to be of particular societal importance. Slope and cliff stability, resistance to slip on earthquake producing faults, and streambed erosion and sedimentation patterns, for example, all depend on an essential phase transition in granular flows from dense, slow moving flows to faster, ultimately more dilated flows. The end-member phase regimes in granular flow have been the subject of some study, but the transition between the two is not well understood. This transitional phase regime, however, can occur over several orders of magnitude of pressure and velocity conditions. Understanding more precisely under what conditions and in what form this transitional phase regime will occur is especially important to understanding geologic events of societal relevance.

Furthermore, the majority of theoretical and experimental granular physics has focused on idealized round, smooth, spherical particles. This work has been essential in establishing the field, but has proven insufficient to describe systems made up of non-spherical particles. Geologic materials are almost never spherical, and hazard events of the greatest violence, such as rock falls or earthquake rupture, actually involve quite angular and rough grains. Static and low velocity shear experiments have found considerable differences in strength and packing patterns of angular granular materials compared to spherical granular materials, but we lack a more precise estimate of how these differences translate into frictional strength of such materials, for example. We also need to understand how these difference carry into transitional and high velocity phase regimes.

Finally, geologically relevant granular materials can be composed of any number of minerals exhibiting a wide range of material properties. The largest influence on the overall rheology of a granular flow is how energy is dissipated in the material. For this reason, properties like yield strength, elastic moduli, and grain fracture criteria play a meaningful role in granular shear flow physics. Until now, however, there has been no experimental or theoretical exploration of the relative importance of these characteristics in the range of geologically relevant materials. Such studies are necessary to accurately describe granular processes occurring in nature and improve hazard models of events in different parts of the world.

Integrating an understanding of the effects of different material properties and grain shape into velocity phase regimes will allow for a complete energy balance to

be drawn up for granular shear flow. Such an understanding will result in effective predictions of rheological behavior based on certain material characteristics and boundary conditions and will answer an enduring and fundamental physics question of how energy entering into a granular system is dissipated.

In Chapter 1, I develop a new method for measuring fluctuation energy in granular shear flows. For high velocity, gas-like flows, a granular temperature paradigm has proven useful. In analogy to kinetic theories, granular temperature is defined as

$$T = \left\langle \frac{1}{2} m \delta v^2 \right\rangle \tag{1}$$

where m is the particle mass and δv is the difference between instantaneous velocity and mean flow velocity. Following kinetic theory, temperature can be directly related to quantities like pressure and viscosity. However, complications in the granular system that are absent at the molecular level make prediction of granular temperature for a particular system difficult. Experimental measurements are required to resolve how energy is transferred between work applied to the system, granular temperature and mean flow characteristics. I show that acoustic energy captures the anticipated behavior of granular temperature as a function of grain size in quartz sand shear flows. I also find that granular temperature (through its proxy acoustic energy) is nearly linearly proportional to inertial number, and dilation is proportional to acoustic energy raised to the power 0.6 ± 0.2. This demonstrates the existence of a relationship between granular temperature and dilation. It is also consistent with

previous results on dilation due to externally imposed vibration, thus showing that internally and externally induced vibrations have identical results on granular shear flows. Incorporating granular temperature into dense shear flows promises a route into studying the transitional regime that is critical to geological systems.

In Chapter 2, I capitalize on the insights of Chapter 1 to explore how internally induced vibrations affect the mechanics of transitional flows. As in Chapter 1, I use a commercial torsional rheometer with an accelerometer attached to measure dilation and acoustic energy output with shear velocity under constant pressure for a sample of angular quartz grains. Image analysis allows me to compare these measurements with the velocity profile within the flow down to the depth of mobilization. As recoverable dilation at the top of the flow is observed with increasing shear velocity, there is simultaneously a recoverable lowering of the depth of mobilization of the flow due to entrainment of lower grains. The velocity profile with depth in the flow is sensitive to driving velocity in both the slowest moving regime of flow near mobilization depth and in the transitional velocity regime. Both of these changes in regime behavior with driving velocity appear to be consequences of the increase in acoustic energy produced by the fastest moving grains in the flow. Separate experiments show that compaction can occur as a result of internally induced noise and externally applied vibration. The amount of compaction observed in these high velocity shear experiments matches that predicted by previous experiments measuring compaction resulting from vibrational energy. In high velocity shear flows, the acoustic energy resulting from grain-grain collisions at the

top of the flow are of high enough amplitude to cause (a) compaction of transitional velocity grains and (b) slightly reduced friction between the lowest-velocity grains that will induce easier entrainment and thus a steepening of velocity depth profile. Consideration of this flow as purely inertial due to its driving velocity would result in an incorrect prediction of its rheology, and consideration of the lower velocity regimes within the flow as operating independently of the faster moving grains above would also be incomplete.

In Chapter 3, I use the tools developed in Chapter 1 in order to explore how the effect described in Chapter 2 is dependent on the material properties of the solid grains. Natural granular flows have a variety of compositions with a wide range of material properties. As the study of granular physics matures, it is important to establish experimentally which material properties are important controllers on flow behavior. I perform dense shear flow experiments with an array of mineral sands designed to test a suite of material properties in order to establish what combination of parameters is the best predictor of differences in flow behavior. Shearing samples from 50 – 300 rad/s under constant pressure of 3.5 kPa, I record dilation and acoustic energy of the shear flow. At inertially-dominated shear velocities, dilation of a granular flow depends on fluctuation energy. Because of a variety of dissipative processes in granular flows, observed dilation often does not vary with observed fluctuation energy, so I compare how these variables differ for each of the five mineral sands tested. Using acoustic energy as a measurement of fluctuation energy, the best predictor of separation between dilation and acoustic energy is the

characteristic length of plastic displacement, δ. As an indicator of a material's propensity to absorb energy through plastic damage or release energy through fracture, this new metric is useful for understanding energy partitioning in granular flows.

With this dissertation I developed experimental methods and produced and analyzed experimental data sets that will further the field of fundamental granular physics. More than that, I have sought to examine existing theories and push the field towards subjects and methodologies most relevant to the earth sciences. I have established that the complications presented by irregular shape, mixed grain size and differences in material fracture properties result in deviations from granular flow theory that relies on descriptions of smooth spheres. I have purposely focused on geologically relevant samples and methods with the hope that understanding energy dissipation in granular shear flows where we have good control on mineralogy, shear zone thickness, shear zone pressure and acoustic radiation will greatly improve rheological modeling of hazard systems like earthquake damage zones and landslides.

Chapter 1

Granular temperature measured experimentally in a shear flow by acoustic energy

Introduction

Granular flows are ubiquitous in nature, yet defy easy characterization or simple rheological laws. A major unresolved question is how instantaneous variations from the mean velocity contribute to the effective rheology of a granular material. In non-granular solids, liquids and gases, fluctuations of a given characteristic are often separated in scale from the mean field. In granular flows, however, fluctuations are of the same scale as the mean flow and therefore integral to all stress responses.

One strategy to quantify and interpret the fluctuation behavior is by characterizing a flow in terms of the granular temperature. In analogy to kinetic theories, granular temperature is defined as

$$T = \left\langle \frac{1}{2} m \delta v^2 \right\rangle \qquad (1)$$

where m is the particle mass and δv is the difference between instantaneous velocity and mean flow velocity (Brilliantov & Pöschel, 2004; Ogawa, 1978). Like in atomic-scale theories, granular temperature is a measure of the kinetic energy of fluctuations,

but it is separated by orders of magnitude from thermodynamic temperature. The transfer of energy between granular temperature (i.e. fluctuation energy) and aspects of the mean flow remains one of the enduring challenges of granular mechanics (Liu & Nagel, 1998).

The application of kinetic theory to granular materials was preceded by the early dimensional analysis work done by Bagnold in 1954 (Bagnold, 1954), which suggested a relationship between pressure, grain size, shear strain rate and solid volume fraction for a granular flow according to the relationship:

$$P \sim f(\phi)\rho_g d^2 \dot{\gamma}^2 \tag{2}$$

where pressure (P) scales with a function, f, of packing fraction (ϕ), particle density (ρ_g), grain diameter (d), and shear strain rate ($\dot{\gamma}$). Later work extended this analysis, showing that both packing fraction and flow friction are dependent on the dimensionless inertial number, I, defined as a ratio of the characteristic timescale for a grain to push down into the flow layer below it (t_{micro}) over the characteristic timescale for a grain to shear over and completely past the grain below it in the direction of flow (t_{macro}) (Andreotti, Forterre, & Pouliquen, 2013; Campbell, 2006; Hill & Yohannes, 2011; Jop, Forterre, & Pouliquen, 2006),

$$I = \frac{\dot{\gamma} d}{\sqrt{P / \rho_g}} . \tag{3}$$

Bagnold's relationship between pressure and volume and consideration of individual particle interactions is reflective of the ideal gas relationship of $PV=nRT$. The idea of a granular temperature, defined as the fluctuation energy of individual grains within a

flow, grew as the basis of a kinetic theory of granular flow (Haff, 1983; Jaeger, Nagel, & Behringer, 1996; Ogawa, 1978).

The granular temperature paradigm has proven useful, particularly to studies of high velocity, gas-like flows referred to as granular gases. Following kinetic theory, temperature can be directly related to quantities pressure and viscosity (Andreotti et al., 2013; Campbell, 1990). However, complications in the granular system that are absent at the molecular level make prediction of granular temperature for a particular system difficult. It is not clear how input energy is partitioned between granular temperature and mechanical work. For a granular gas (compared to a molecular gas) there is an additional dissipative loss of energy in particle collisions as a result of granular mass, friction, strength and shape (Andreotti et al., 2013; Brilliantov & Pöschel, 2004; Jaeger et al., 1996; van der Elst, Brodsky, Le Bas, & Johnson, 2012). These dissipative effects are increasingly important and unresolved as granular flows transition to denser, liquid-like flows where collision rates increase. Experiments are needed to clarify the relationship between granular temperature and the driving forces for realistic systems over a range of velocities encompassing this transition.

Outside of numerical simulations, experimental estimations of granular temperature have relied on interpretations of the effects of granular temperature on a flow rather than direct measurements. The only extant methods of inferring granular temperature are through image analysis and acoustic monitoring.

Visual techniques for observing fluctuation velocities are limited by technology and often require use of 2D materials or method-specific granular composition (Bocquet et al., 2001; Warr et al., 1995). Dense shear flows are particularly difficult to study visually (Yates & Simons, 1994). These experimental limitations have limited our understanding of how energy input into a granular flow partitions into shear flow on the one hand and fluctuation energy, i.e. granular temperature, on the other hand.

Significant progress has been made using passive acoustic emissions to monitor industrial processes involving granular materials. Frictional slip and particle collision can produce acoustic energy resonating at the scale of both individual grains and force chain assemblies (Michlmayr & Or, 2014), and frequency and amplitude information from these signals has been used to distinguish fluidized bed regimes (Cody et al., 1996; Jingdai et al., 2009) and measure grain characteristics during granulation processes (Jiang et al., 2007; Leach et al., 1977; Leach et al., 1978; Tsujimoto et al., 2000). In geology, acoustic emissions have been used to monitor grain breakage and force chain reorganization in granular material under compaction and slow shear (Johnson et al., 2013; Karner et al., 2003; Mair et al., 2007). Field and laboratory investigations have connected "booming sand dune" frequencies to shear zone separation and internal dune structure (Hunt & Vriend, 2010; Tan et al., 2015; Vriend et al., 2007) or grain diameter and shear rate (Andreotti, 2004; Dagois-Bohy & Pont, 2012; Douady et al., 2006).

The success of acoustic energy measurements as a proxy for granular temperature in gas fluidized beds (Cody et al., 1996) has suggested that it may be a useful measure in shear systems as well. Acoustic monitoring of sheared granular material has confirmed a relationship between acoustic emissions and driving shear velocity at low velocity (Andreotti, 2004; Douady et al., 2006; Mair et al., 2007; Michlmayr & Or, 2014) but has not been used as a probe for granular temperature in high velocity dense shear flows. In such flows the role of granular temperature is less clear than in grain inertial regimes where velocity fluctuations are more isotropic, which generally occur in less dense flows and flows made up of perfectly elastic grains (Campbell, 2006). Dense, sheared granular flows are famously anisotropic, yet fluctuations may still play a role in their flow (Andreotti, 2004; Ferdowsi et al., 2015; van der Elst et al., 2012). Elucidating this role is the goal of this paper.

We conducted a new set of controlled pressure experiments in the high shear velocity grain-inertial regime, also known as the granular gas regime. We were simultaneously able to measure volume changes of a granular flow over a range of shear velocities as well as fluctuation energy directly through acoustic output of the flow.

In a dense, controlled-pressure granular flow, high velocity granular gases are dominated by inertially driven grain-to-grain collisions (Campbell, 2006). The magnitude of fluctuation of energy within a flow is determined by these grain-to-grain collisions, as deviations of instantaneous velocity from mean velocity will

depend on difference in grain velocities before and after collisions (Cody et al., 1996; Michlmayr & Or, 2014). Kinetic energy released during an individual collision is

$$KE = \frac{1}{2}mv^2 \tag{4}$$

where m is particle mass and v is the difference in particle velocity before and after collision. The strongest collisions will involve particles moving at the maximum fluctuation velocity, and the minimum fluctuation velocity will occur at the midpoint of collision.

For this study, we first assess if acoustic energy output accurately measures kinetic energy fluctuations of a granular shear flow—and thus granular temperature. We then present measurements of dilation and acoustic energy collected over an order of magnitude of inertial numbers in order to evaluate how energy is transferred from granular temperature to mechanical work in the form of flow dilation.

To test the consistency of acoustic energy measurements with predictions of granular temperature, we compared the scaling of acoustic energy with different grain masses subjected to the same shearing velocities. We used four grain size ranges from the same granular material (same particle density ρ_g), therefore acoustic energy during flow should scale with grain volume ($m \sim \rho_g d^3$).

This is the first experiment to simultaneously measure granular temperature via acoustic energy in a dense shear flow and flow dilation over an order of magnitude of shear velocities under constant pressure. The full set of results shows strong relationships between acoustic energy, inertial number and flow volume that held for multiple samples over a range of grain sizes between 125-500 microns in

diameter. Understanding how energy is partitioned between dilation and granular temperature during the flow of granular materials is fundamental to addressing the questions raised by kinetic theory of granular gases.

Experiments and Methods

We tested samples using a TA Instruments AR2000ex torsional rheometer to measure volume changes in granular samples as they were sheared while maintaining constant pressure (Figure 1), after the design used by van der Elst et al., 2012 and Lu et al., 2007.

Experimental Apparatus

A 19 mm diameter steel rotor fits inside a glass jacket with approximately 10 μm clearance between the rotor edge and the jacket (Figure 1). The glass jacket is epoxied to a flat aluminum plate, which is attached to a temperature-controlled Peltier plate, set to 25°C.

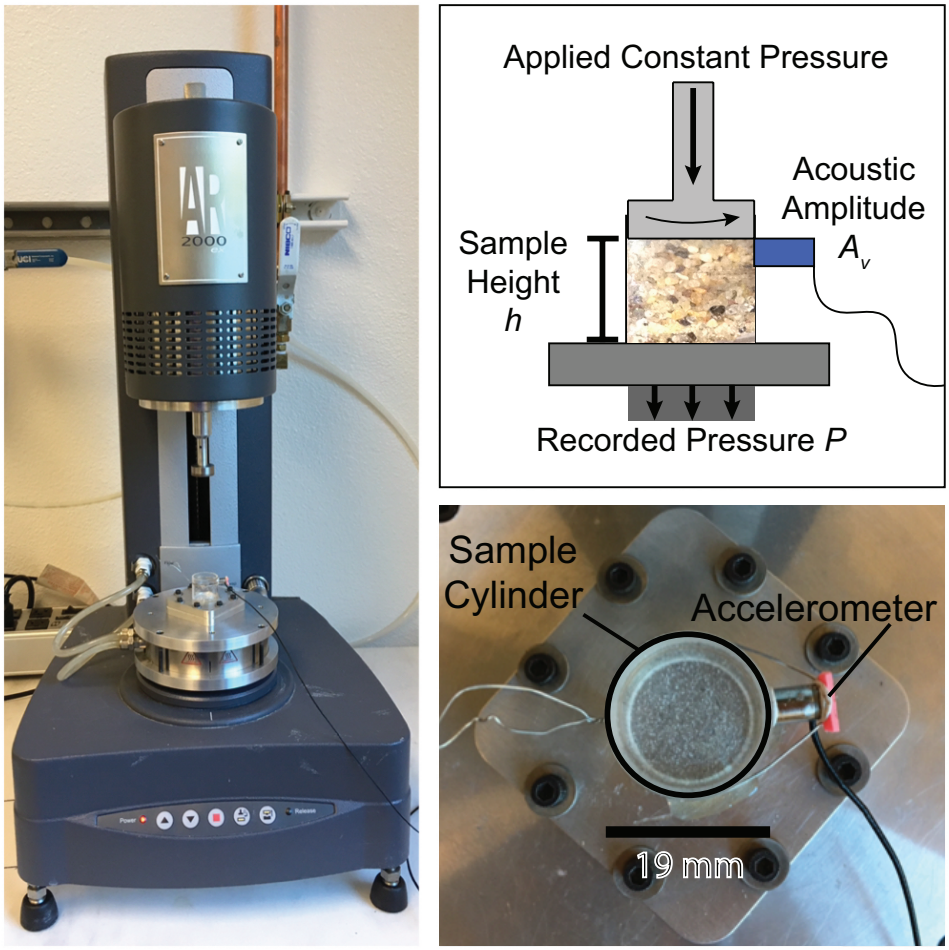

Figure 1: Photographs of rheometer and experimental set up. (left) TA Instruments AR2000ex torsional rheometer with custom rotor and sample cylinder attached. (top right) Schematic of experimental configuration showing variables that were measured. (bottom right) Sample cylinder has a Bruel & Kjaer charge accelerometer attached to the outside of the glass at the shear zone level using museum putty and secured with a wire.

We use the TA Instruments AR2000ex rheometer's internal software to maintain a constant axial force of 1 N, exerting an axial stress of 3.5 kPa on the granular sample. At this axial stress, we are able to focus the investigation on grain-to-grain interactions in the absence of widespread grain breakage or comminution. To

maintain a constant normal force, the height of the rotor adjusts to compensate for sample compaction (weakening) or dilation (strengthening). In this way we measure change in sample height (Δh) with shear strain rate ($\dot{\gamma}$) under constant normal stress (P).

Acoustic emissions result in acceleration of the apparatus that are recorded using a Bruel & Kjaer 4373 charge accelerometer coupled to the outside of the glass jacket at the level of the shear zone. Acceleration amplitude is recorded in volts (A_v) at 200kHz sampling frequency. Since in this study we focus on relative measurements of acoustic energy and calibration of the accelerometer to absolute motion is complex (McLaskey et al., 2015), we report our acceleration measurements in the laboratory units, i.e., volts.

We can define an effective acoustic energy using the laboratory units by assuming that the glass jacket to which the sensor is attached is elastic, and thus that measured acceleration is linearly related to displacement at a given frequency. Wave amplitude squared is a measure of the energy of the signal. We define the laboratory measurements of acoustic energy per grain as

$$E_a = \frac{\left\langle A_v^2 \right\rangle}{N_s} \tag{5}$$

where the angular brackets indicate an average of the data over a fixed time window, and N_s is the number of grains in the top, fastest moving layer touching the glass cylinder. Collisions between these fast moving outer-most grains will be most likely to contribute to the measure acoustic energy. For this study we use a time window of

0.1 s and have verified that our results are robust to time window choices between the sample interval and 1 s.

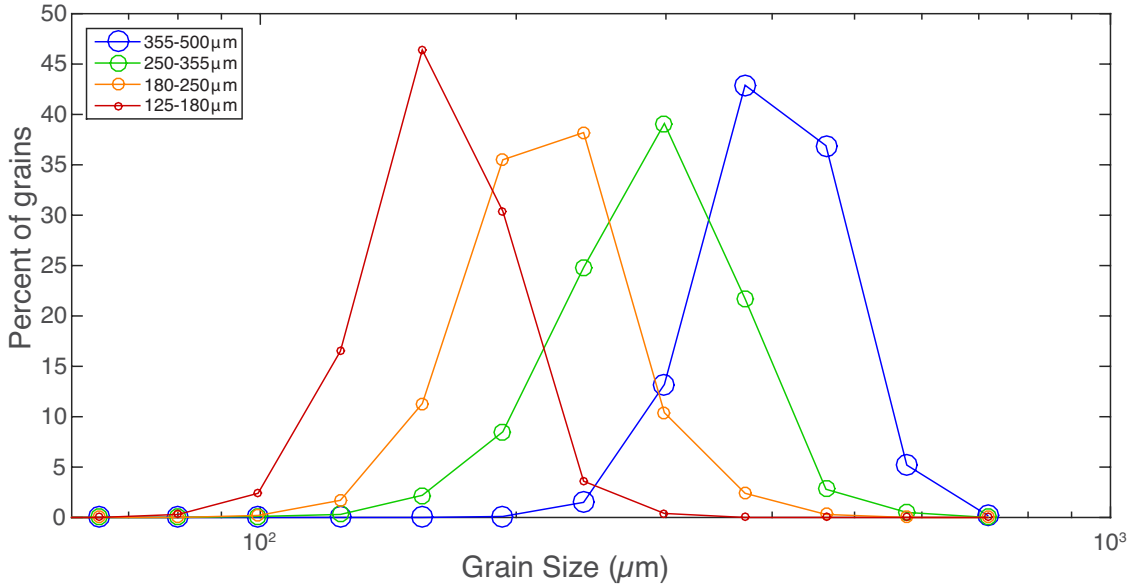

Figure 2: Grain size distributions are shown for four size ranges of quartz beach sand from Natural Bridges Beach and Cowells Beach in Santa Cruz, CA. Grain size was measured using a Retsch Technology Camsizer Particle Analyzer.

Sample Preparation

We collected angular granular samples from Natural Bridges Beach and Cowells Beach in Santa Cruz, CA. To minimize mineralogical variability, we used a Frantz Magnetic Separator to remove ferromagnetic and paramagnetic grains, leaving mainly quartz, feldspar and a small amount of calcite sand. Mineralogy was determined from a combination of visual inspection and Raman spectrometry. The makeup by number of grains was 86% quartz, 12% feldspar, 1% calcite, and 1% other. We sieved the samples into four logarithmically sized grain diameter ranges:

125-180 μm, 180-250 μm, 250-355 μm and 350-500 μm. Figure 2 shows the size distributions within these four samples, measured using a Retsch Technology Camsizer Particle Analyzer.

Experimental Procedure

Each sample was conditioned prior to data collection using the following protocol:

1x	3600s at $1x10^{-3}$ rad/s
1x	650s continuously increasing velocity 25 rad/s – 300 rad/s 650s continuously decreasing velocity 300 rad/s – 25 rad/s
9x	1000s continuously increasing velocity 25 rad/s – 300 rad/s 1000s continuously decreasing velocity 300 rad/s – 25 rad/s

In order to measure the granular samples as close to steady state as possible at a given velocity, conditioning of the sample was required to minimize the contribution of long term settling of the sample as it shears. Figure 3a and 4a show changes in sample height and acoustic energy, respectively, throughout the conditioning cycles.

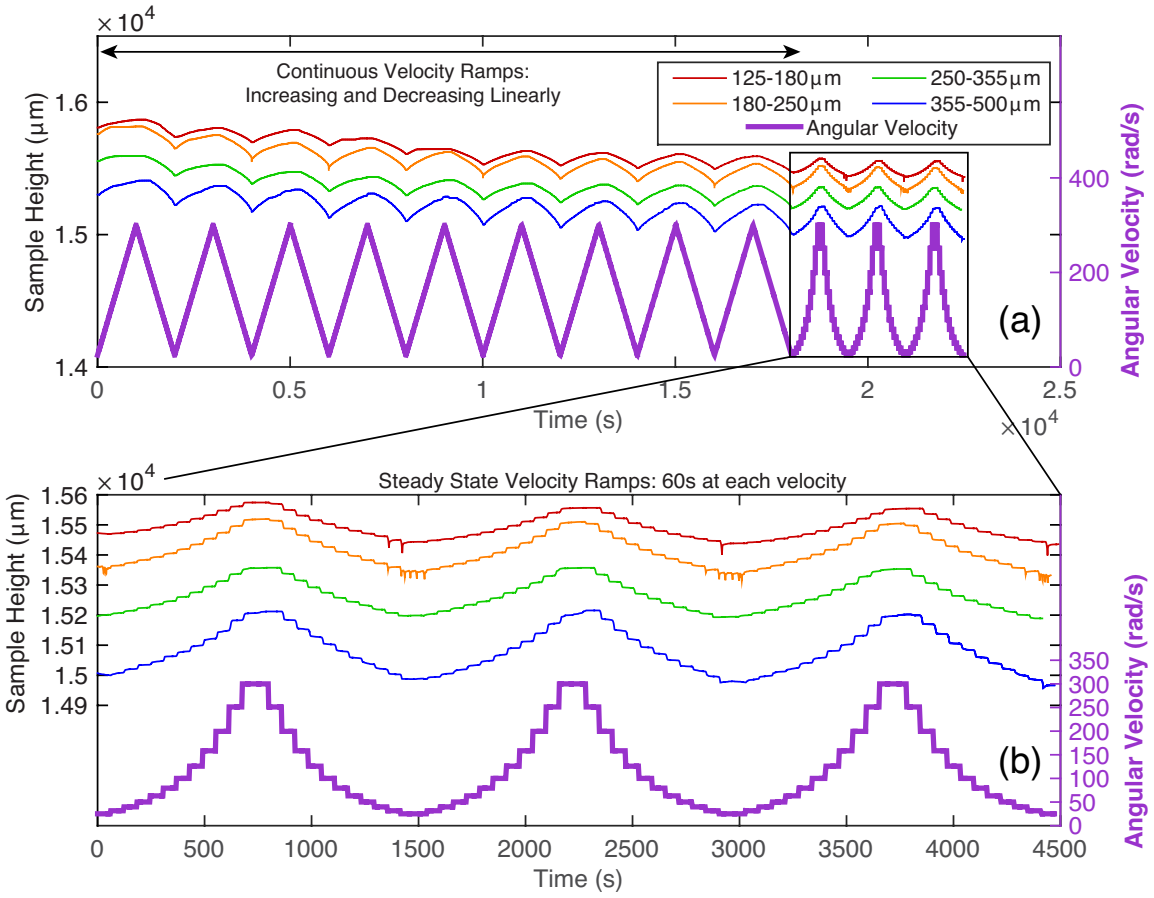

Figure 3: Sample thickness as a function of experimental time for all four size ranges of samples tested (blue representing the largest, green the second largest, orange the second smallest, and red representing the smallest). (a) shows full conditioning cycles and data collection. (b) shows just data used in analysis, collected after conditioning.

Data used for analysis from the steady state stepped velocity ramps was collected after conditioning was complete using the following protocol:

3x stepwise increasing velocity from 25 rad/s – 300 rad/s and decreasing velocity from 300 rad/s – 25 rad/s in 24 logarithmically spaced velocity steps, held for 60s each

With the axial force controlled at 1 N, rotor height was measured at logarithmically spaced velocity steps between 25 rad/s and 300 rad/s. Each velocity was held for 60 s

to achieve steady state. Rotor height, shear strain rate, and axial force were recorded at 1 Hz sampling frequency, and the first 30s of each velocity step was ignored during analysis so that only steady state data were used in evaluation. Data were recorded at steady state for a given velocity, and results are reversible, meaning the rotor height did not change for a given velocity step whether the overall velocity ramp direction was moving from slow to fast or from fast to slow.

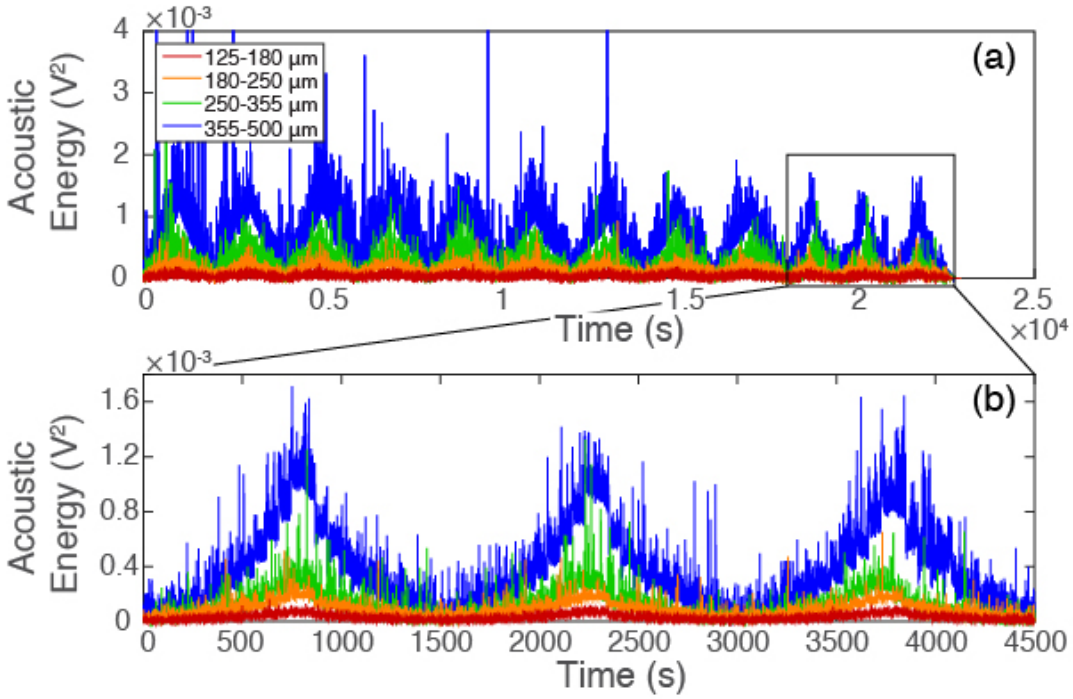

Figure 4: Acoustic energy (acoustic amplitude measured in volts, A_v (V), squared) is shown with experimental time. (a) shows full experiment including conditioning cycles. (b) shows final data used for analysis. Shown here is the mean of acoustic energy averaged per 0.1s of collected data.

Over the course of conditioning the samples, compaction occurred with each subsequent linearly increasing-and-decreasing continuous velocity step. The rate of this long-term compaction during conditioning reduced by the end of the 11

conditioning cycles, as shown in Figures 3a and 4a. By the end of conditioning, the sample height did not change significantly between ramps, such that the sample height at a given velocity was the same as the sample height at that velocity in different ramp, regardless of timing or direction (i.e. increasing or decreasing). Figures 3b and 4b show this reversibility and repeatability for sample height and acoustic energy respectively. Acoustic energy decreased with the number of conditioning steps as the sample settled into a repeatable orientation, and acoustic energy was repeatable and reversible for the final three steady state stepped velocity ramps (see Figure 4b).

Error Analysis

There are two main sources of potential uncertainty in the change in sample height (Δh) measurements. One is the spread in height measurements over the course of a steady state velocity step, but this range is usually small. The second, and larger, source of uncertainty in Δh is associated with the critical sample height (h_0) to which the measured sample height (h) is compared in order to calculate change in sample height.

Absolute shear zone thickness measurements do not have sufficient precision because the base of the shear zone is not well-determined. For these experiments, the stress is controlled but the volume is not, and each experiment is begun with more sand in the sample cylinder than will ultimately be integrated into the shear zone. Therefore we find Δh relative to the low velocity, steady-state critical sample height

(h_0). Critical height is defined as the height of the sample when flowing at inertial numbers below 10^{-4} (Figure 5), and then average dilation for all grain sizes above this height at angular velocity ω=100 rad/s (I=0.17; solid black line in Figure 5) was found to be $h_{100} = 0.33 \pm 0.075$ grain diameters.

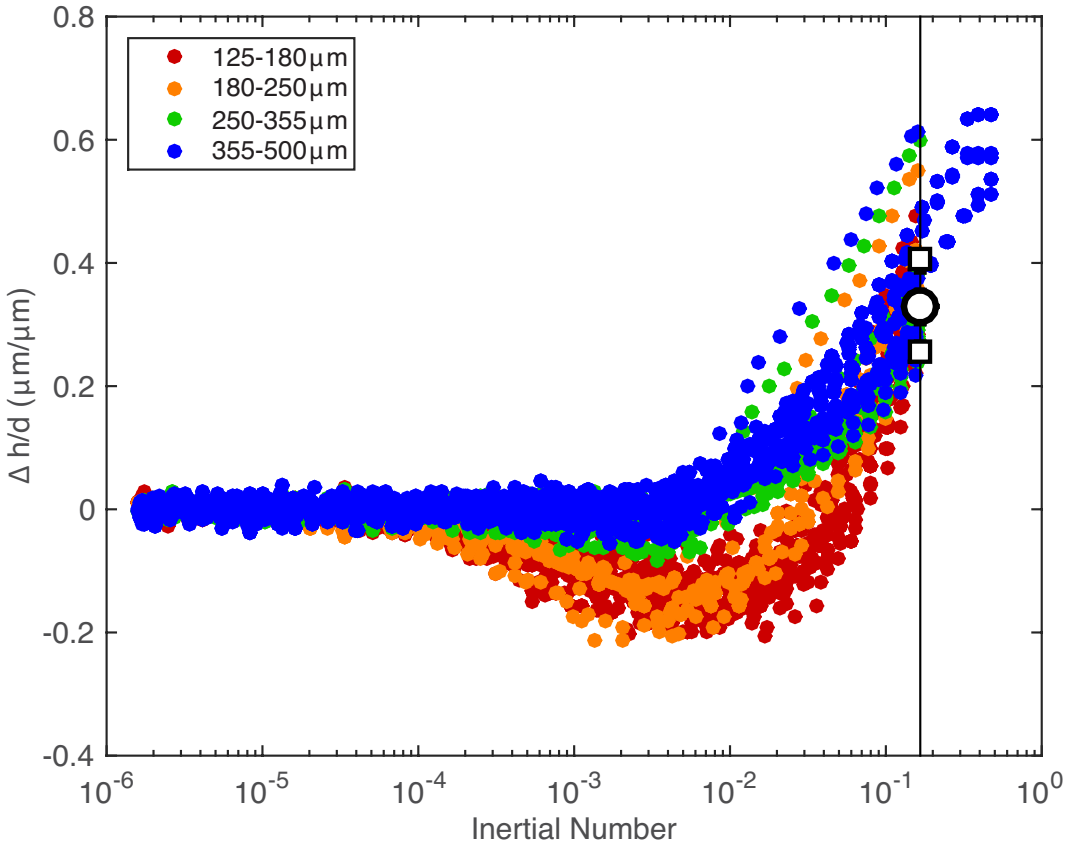

Figure 5: Black line shows inertial number for angular velocity ω=100 rad/s (I=0.17). White circle marks the mean dilation above the lowest velocity quasi-static height, as observed in low shear velocity tests plotted here. Mean sample height for all grain sizes at 100 rad/s shear velocity is 0.33 +/- 0.075 grain diameters.

Measured steady state heights (h) shown in Figure 3b were zeroed to the sample height during the first 100 rad/s velocity step, and then 0.33 grain diameters was added to all height measurements in order show Δh. The standard deviation of

h_{100} as measured in Figure 5, 7.5 x 10^{-2} grain diameters, was then propagated into the error for all Δh.

Results

We now combine the recorded acoustic, velocity, volume and axial force data to address two key issues. First of all, we will examine whether the acoustic records tracks a quantity that can be reasonably interpreted as a proxy for granular temperature. We will then examine the interrelationships between recorded acoustic energy, dilation, and a parameter that captures the overall dynamic statement of the system, i.e., inertial number.

Fits were calculated based on data collected at angular velocities above 50 rad/s only, because these higher shear velocities returned more consistent results with lower error than data collected at lower shear velocities, implying the flow above 50 rad/s is more firmly in the granular gas regime and thus of most interest for this study.

Acoustic Energy as a proxy for granular temperature

If acoustic energy recorded during granular flow is representative of fluctuation energy caused by grain-to-grain collisions, then at a given shear strain rate, the acoustic energy should scale with grain mass (eq. 4). Figure 6 shows that the acoustic energy generated by the four grain size ranges collapse onto each other when normalized by grain diameter cubed.

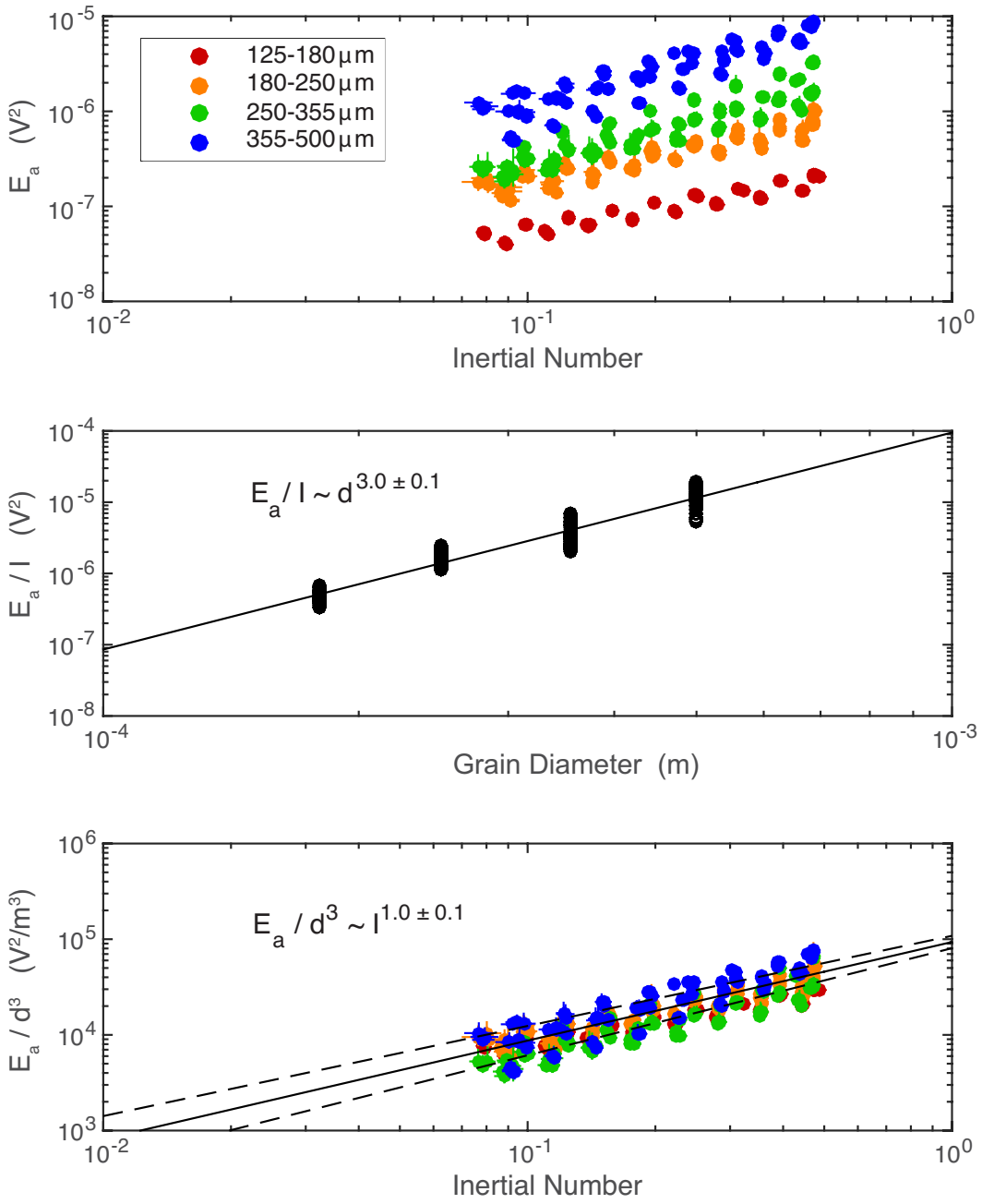

Figure 6: (Top) Acoustic energy per grain (E_a) for four grain sizes scale nearly linearly with inertial number for each. (Center) Acoustic energy per grain normalized by inertial number (E_a/I) scales with grain diameter (d) cubed. (Bottom) Acoustic energy per grain normalized by grain mass, i.e. grain diameter cubed (E_a/d^3) as a function of inertial number (I). Solid lines show fit to all grain sizes and dashed lines show 95% confidence intervals.

The radial shear apparatus creates a radial velocity gradient with the fastest shear occurring at the edge of the rotor and the slowest occurring at the center. As a result of this gradient, sand grains under shear will exhibit size segregation, with the largest grains moving towards the faster shear rates and the smaller grains moving towards the slower shear rates (Cantelaube & Bideau, 1995; Savage & Lun, 1988). Therefore the grains at the outer edge nearest the sensor will be the largest grains in the sample. Thus when considering normalizing by grain mass we normalize by the maximum sieve mesh grain size cubed. The consistency of the measurements with the predicted grain size scaling confirms that acoustic energy is a good proxy for the kinetic energy of collisions (granular temperature).

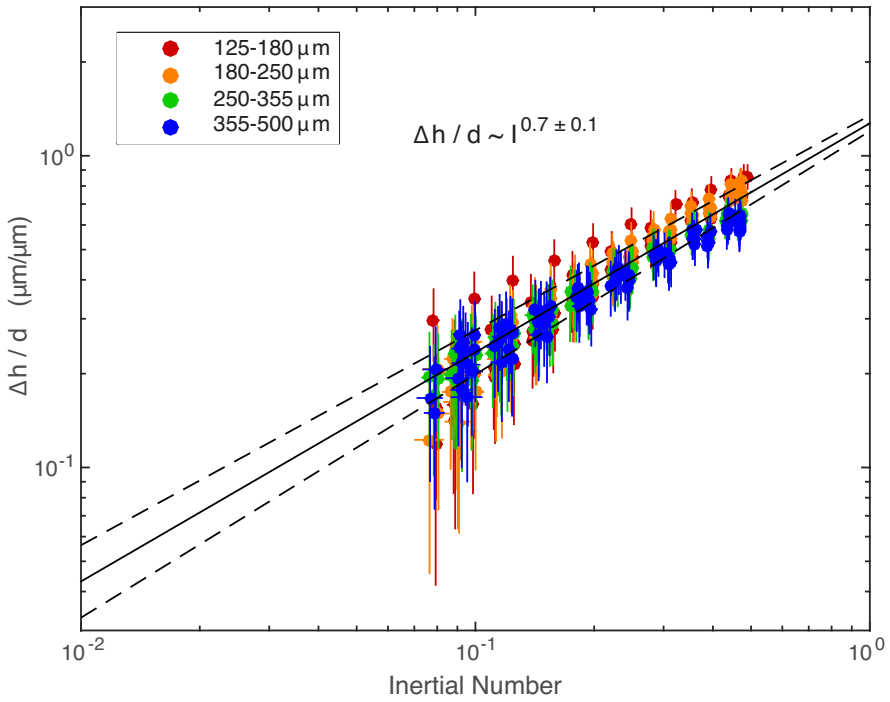

Figure 7: Relative change in sample thickness normalized by median grain diameter (Δh/d) scales with inertial number (I) to the power 0.7 with 95% confidence interval ±0.1. Solid lines show fit to all grain sizes combined and dashed lines show 95% confidence intervals.

Inertial number and acoustic energy

For analysis of the dynamics we use the inertial number (eq. 3), which takes pressure and shear strain rate into account, allowing for comparison across different experimental geometries or natural circumstances. For each 60 s velocity step, inertial number varies primarily with variations in the applied axial force, which, although controlled by the rheometer at 1 N, does vary in practice with a standard deviation of ±0.15 N over the final 30 s of analyzed velocity steps.

For each grain size tested, change in acoustic energy scales linearly with inertial number, and these relationships collapse onto each other for all grain sizes when normalized by grain mass (Figure 6). Averaged across all four grain size ranges, the relationship observed is:

$$\frac{E_a}{d^3} \sim I^{1.0\pm0.1} \tag{6}$$

Dilation as function of inertia number and acoustic energy

Relative sample height is calculated based on the average number of grain diameters above minimum sample height (also known as critical height) at 100 rad/s (i.e. lowest velocities tested in these trials) as measured in previous low velocity experiments. Variation in the sample height at a given shear velocity is the result of both the distribution in measured gap height over the final 30 s of an individual 60 s velocity step and the uncertainty surrounding the average number of grain diameters above the minimum sample height at 100 rad/s. Figure 7 shows the following

observed relationship between sample height normalized by grain diameter and inertial number:

$$\frac{\Delta h}{d} \sim I^{0.7\pm0.1} \tag{7}$$

As shown in Figure 8, normalized change in sample height is related to the normalized acoustic energy output by the following relationship:

$$\frac{\Delta h}{d} \sim \left(\frac{E_a}{d^3}\right)^{0.6\pm0.2} \tag{8}$$

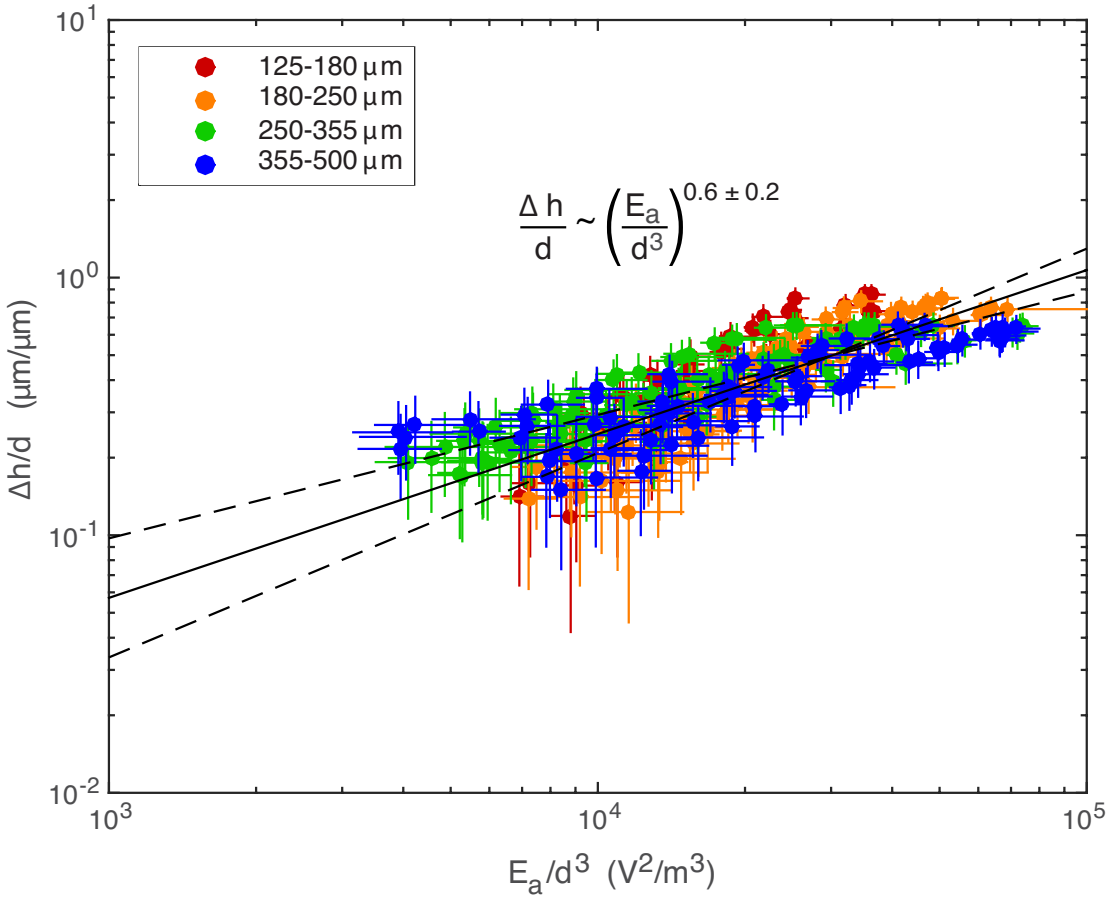

Figure 8: Change in sample height normalized by grain diameter with recorded acoustic energy per grain normalized by grain mass. Fit calculated for all grain sizes. Solid line shows fit to all grain sizes combined as identified by the equations and dashed lines show 95% confidence intervals.

This difference in relationship between equations 6 and 7 shows that the energy put into the flow (via applied shear stress which results in a given inertial number) is partitioned unequally into granular temperature and dilation of the flow.

Interpretation

The controlled pressure experiments described here show that acoustic energy recorded during granular flow at inertial numbers between 0.1 and 1 scales with grain mass. Results showed a linear relationship between acoustic energy and shear flow velocity as well as a strong power law relationship between shear zone dilation and flow velocity.

At high shear velocities, a granular flow is thought to behave like a gas, with grains supporting applied shear stress through binary collisions and exchanges of inertia. The scaling of acoustic energy with grain mass is consistent with its proposed representation of energy released in grain collisions. Recorded acoustic energy normalized by grain mass varies nearly linearly with inertial number (and thus shear velocity for these experiments) for all grain sizes, and this relationship strengthens as velocity increases and inertial number approaches 1.

Collision rate determines fluctuation energy in a granular flow. Inertial number in these experiments is controlled by varying shear rate. If, in a granular gas regime, a grain in an overlying layer collides with each grain in an underlying layer in the course of passing over it, it follows that collision rate and thus granular temperature and shear rate will coincide (Andreotti, 2004).

These experiments are compatible with previous experimental studies of granular gas temperature based on visual measurements vibrated but unsheared granular material. Warr et al., 1995 observed a relationship of

$$\Delta h_{cm} \sim E_0^{0.72\pm0.04} \tag{9}$$

where Δh_{cm} is change in the height of the center of mass of the granular mixture and E_0 is granular temperature. Temperature in those experiments was calculated by fitting the bulk speed distribution function as captured by 1000 fps digital camera images. Importantly, Warr et al.'s granular temperature was induced by applied vibrations, whereas the granular temperature recorded here was internally induced during shearing of the flow over an order of magnitude of shear velocities. The naturally produced granular vibrations are observed to exert an amount of mechanical work in the form of flow dilation that is consistent with the vibration-to-dilation transfer of energy observed in Warr et al.'s stationary case.

This demonstrates that whether internally induced during shear flow or externally applied, vibrations in granular matter produce identical amounts of dilatation, indicating the centrality of granular temperature to granular matter rheology, including dense shear flows. Although the import of granular temperature has long been appreciated in dilute flows and externally vibrated media, the significance for dense shear flows has been less appreciated.

The ability to produce vibrations internally in a shear flow combined with the observed consistency in dilation as a function of acoustic energy suggests that the suite of rheological behavior associated with vibration may have implications in shear

flows. Weakening, dilation and, under appropriate conditions, compaction, are all associated with vibration and therefore may occur in shear flows as wells due to the internally produced vibrations (Lu et al., 2007; van der Elst et al., 2012).

Conclusions

The acoustic energy output of a granular flow is a direct measurement of fluctuation energy of the flow, which provides a window into how energy input into the flow through controlled pressure and shear velocity is partitioned into granular temperature, as well as how granular temperature relates directly to volume change in these experiments.

The measured granular temperatures show the transition from liquid to gas. Historically, inertial number I is usually used for granular liquids, granular temperature usually used for gases, but in these experiments there is a relationship between the two, and at this transitional velocity flow is both liquid and gaseous at different points locally in the same flow (regions of expansion in bulk liquid). Normally liquid and gas phases of a granular flow are described separately; here there is a linear relationship. This relationship is a consequence of the fact that the flow is a composite of the liquid and gas phases of granular flow.

We recover specific relationships between granular temperature (through its proxy acoustic energy), dilation and inertia number. Dilation (change in grain height) normalized by grain size scales as $E_a^{\,0.6 \pm 0.2}$ and $I^{\,0.7 \pm 0.1}$. Granular temperature for these steady-state experiments is a function of mechanical energy input with

$E_a \sim I^{1.0 \pm 0.1}$. The results show that the vibrations produced internally as a natural part of the shear flow produce similar dilation as forced vibrations in stationary flow, suggesting that internally produced vibrations are an important aspect of understanding and predicting the behavior of shear flows (van der Elst et al., 2012).

Agreement with previous laboratory measurements of granular temperature confirms the suitability of acoustic energy to represent fluctuation velocity of a granular flow. The experiments show that acoustic energy shows great promise for measuring the internal, granular temperature in laboratory experiments.

References

Andreotti, B. (2004). The Song of Dunes as a Wave-Particle Mode Locking. *Physical Review Letters*, *93*(23), 238001. http://doi.org/10.1103/PhysRevLett.93.238001

Andreotti, B., Forterre, Y., & Pouliquen, O. (2013). Granular Media: Between Fluid and Solid. New York: Cambridge Univ Press.

Bagnold, R. A. (1954). Experiments on a Gravity-Free Dispersion of Large Solid Spheres in a Newtonian Fluid under Shear. *Proceedings of the Royal Society a: Mathematical, Physical and Engineering Sciences*, *225*(1160).

Bocquet, L., Losert, W., Schalk, D., Lubensky, T. C., & Gollub, J. P. (2001). Granular shear flow dynamics and forces: Experiment and continuum theory. *Physical Review E*, *65*(1), 011307. http://doi.org/10.1103/PhysRevE.65.011307

Brilliantov, N. V., & Pöschel, T. (2004). Kinetic Theory of Granular Gases. Oxford: Oxford University Press.

Campbell, C. S. (1990). Rapid granular flows. *Annual Review of Fluid Mechanics*.

Campbell, C. S. (2006). Granular material flows – An overview. *Powder Technology*, *162*(3), 208–229. http://doi.org/10.1016/j.powtec.2005.12.008

Cantelaube, F., & Bideau, D. (1995). Radial segregation in a 2d drum: an experimental analysis. *EPL (Europhysics Letters)*, *30*(3), 133.

Cody, G. D., Goldfarb, D. J., Storch, G. V., & Norris, A. N. (1996). Particle granular temperature in gas fluidized beds. *Powder Technology*.

Dagois-Bohy, S., & Pont, du, S. C. (2012). Singing-sand avalanches without dunes. *Geophysical Research Letters*, *39*(20), L20310.

Douady, S., Manning, A., Hersen, P., Elbelrhiti, H., Protière, S., Daerr, A., & Kabbachi, B. (2006). Song of the Dunes as a Self-Synchronized Instrument. *Physical Review Letters*, *97*(1), 018002.

Jates, J. G. & Simons, S. J. R. (1994). Experimental methods in fluidization research. *International Journal of Multiphase Flow*, *20*, 297–330.

Ferdowsi, B., Griffa, M., & Guyer, R. A. (2015). Acoustically induced slip in sheared granular layers: Application to dynamic earthquake triggering. *Geophysical Research Letters*, *42*(22), 9750–9757. http://doi.org/10.1002/2015GL066096

Haff, P. K. (1983). Grain flow as a fluid-mechanical phenomenon. *Journal of Fluid Mechanics*, *134*, 401–430.

Hill, K. M., & Yohannes, B. (2011). Rheology of Dense Granular Mixtures: Boundary Pressures. *Physical Review Letters*, *106*(5), 058302.

Hunt, M. L., & Vriend, N. M. (2010). Booming Sand Dunes. *Annual Review of Earth and Planetary Sciences*, *38*(1), 281–301. http://doi.org/10.1146/annurev-earth-040809-152336

Jaeger, H. M., Nagel, S. R., & Behringer, R. P. (1996). Granular solids, liquids, and gases. *Reviews of Modern Physics*, *68*(4), 1259–1273.

Jiang, X. J., Wang, J. D., Jiang, B. B., & Yang, Y. (2007). Study of the power spectrum of acoustic emission (AE) by accelerometers in fluidized beds. *Industrial & Engineering Chemistry Research*, *46*(21), 6904–6909.

Jingdai, W., Congjing, R., & Yongrong, Y. (2009). Characterization of flow regime transition and particle motion using acoustic emission measurement in a gas-solid fluidized bed. *AIChE Journal*, *12*(3), NA–NA. http://doi.org/10.1016/S0009-2509(00)00540-6

Johnson, P. A., Ferdowsi, B., Kaproth, B. M., Scuderi, M., Griffa, M., Carmeliet, J., et al. (2013). Acoustic emission and microslip precursors to stick-slip failure in sheared granular material. *Geophysical Research Letters*, *40*(21), 5627–5631.

Jop, P., Forterre, Y., & Pouliquen, O. (2006). A constitutive law for dense granular flows. *Nature*, *441*(7094), 727–730. http://doi.org/10.1038/nature04801

Karner, S. L., Chester, F. M., Kronenberg, A. K., & Chester, J. S. (2003). Subcritical compaction and yielding of granular quartz sand. *Tectonophysics*, *377*(3-4), 357–381. http://doi.org/10.1016/j.tecto.2003.10.006

Leach, M. F., Rubin, G. A., & Williams, J. C. (1977). Particle size determination from acoustic emissions. *Powder Technology*.

Leach, M. F., Rubin, G. A., & Williams, J. C. (1978). Particle size distribution characterization from acoustic emissions. *Powder Technology*.

Liu, A. J., & Nagel, S. R. (1998). Jamming is just not cool any more. Nature.

Lu, K., Brodsky, E. E., & Kavehpour, H. P. (2007). Shear-weakening of the transitional regime for granular flow. *Journal of Fluid Mechanics*, *587*.

Mair, K., Marone, C., & Young, R. P. (2007). Rate dependence of acoustic emissions generated during shear of simulated fault gouge. *Bulletin of the Seismological Society of America*, *97*(6), 1841–1849. http://doi.org/10.1785/0120060242

McLaskey, G. C., Lockner, D. A., Kilgore, B. D., & Beeler, N. M. (2015). A Robust Calibration Technique for Acoustic Emission Systems Based on Momentum Transfer from a Ball Drop. *Bulletin of the Seismological Society of America*, *105*(1), 257–271. http://doi.org/10.1785/0120140170

Michlmayr, G., & Or, D. (2014). Mechanisms for acoustic emissions generation during granular shearing. *Granular Matter*, *16*(5), 627–640. http://doi.org/10.1007/s10035-014-0516-2

Ogawa, S. (1978). Multitemperature theory of granular materials. (S. C. Cowin & S. M, Eds.). Tokyo: Gakujutsu Bunker Fukyukai.

Savage, S. B., & Lun, C. (1988). Particle size segregation in inclined chute flow of dry cohesionless granular solids. *Journal of Fluid Mechanics*, *189*, 311–335.

Tan, D. S., Jenkins, J. T., Keast, S. C., & Sachse, W. H. (2015). Acoustic signals generated in inclined granular flows. *Journal of Geophysical Research: Earth Surface*, *120*(10), 2027–2039. http://doi.org/10.1029/2007GL030276

Tsujimoto, H., Yokoyama, T., Huang, C. C., & Sekiguchi, I. (2000). Monitoring particle fluidization in a fluidized bed granulator with an acoustic emission sensor. *Powder Technology*, *113*(1-2), 88–96. http://doi.org/10.1016/S0032-5910(00)00205-9

van der Elst, N. J., Brodsky, E. E., Le Bas, P.-Y., & Johnson, P. A. (2012). Auto-acoustic compaction in steady shear flows: Experimental evidence for suppression of shear dilatancy by internal acoustic vibration. *Journal of Geophysical Research*, *117*(B9), B09314. http://doi.org/10.1029/2011JB008897

Vriend, N. M., Hunt, M. L., & Clayton, R. W. (2007). Solving the mystery of booming sand dunes. *Geophysical Research Letters*, *34*(16), L16306. http://doi.org/10.1029/2007GL030276

Warr, S., Huntley, J. M., & Jacques, G. (1995). Fluidization of a two-dimensional granular system: Experimental study and scaling behavior. *Physical Review E*.

Chapter 2

The global coupling between inertial and transitional regimes in granular shear flow

Introduction

Granular materials like powders and sands exhibit different rheological phases when exposed to shear. When sheared at low velocity and high pressure, granular materials behave like a solid, and pressure and volume remain independent of shear velocity. At high shear velocities and low pressures, however, these materials are no longer solid-like and can exhibit both a viscous rheology, like a liquid, or a gas-like rheology similar to kinetic theory of molecular gases, where pressure and volume of the material are dependent on a quantity termed kinetic granular temperature (Jaeger et al. 1996). Granular temperature in these scenarios is a measurement of fluctuation energy within the flow, that is, how the instantaneous velocity of any given particle varies from the overall mean velocity of particles in the flow at any moment (Ogawa et al. 1978; Brilliantov & Poeschel 2006).

As shear velocity increases, granular temperature increases as well. Assumptions of how granular temperature changes with shear velocity vary (Ogawa et al. 1978; Jop et al. 2006; Campbell, 2006). Recent experimental work using the

output of acoustic energy from a granular shear flow found that granular temperature varies linearly with shear velocity (Taylor & Brodsky 2017; Cody et al. 1996). Following an analogy to the gas law for molecular gases, $PV=nRT$, it is assumed that under constant pressure, volume of the flow will change linearly with temperature. Previous studies of high velocity shear flows and high temperature static grain packs found that the amount of dilation observed is actually less than linear with granular temperature (Taylor and Brodsky 2017; Warr et al. 1995).

Phase regimes of granular flow are described using the dimensionless inertial number

$$I = \frac{\dot{\gamma} d}{\sqrt{P / \rho}} \quad (1)$$

where $\dot{\gamma}$ is shear rate, d is grain diameter, P is pressure and ρ is material density of the grains. Below inertial numbers of 10^{-3}, a granular flow is solid-like. Granular flows enter the gas-like inertial regime at inertial numbers above a value of about 10^{-1} (da Cruz et al., 2005), and in between inertial numbers of 10^{-3} and 10^{-1} the flow regime is considered transitional. In any system with inherent stress gradients, however, high inertial number gas-like flows will be found directly adjacent to lower inertial number transitional velocity regime flows. Sources of such stress gradients are abundant in natural settings and can include wall friction or irregular or curved shear zone geometries. Although experimental studies of landslides and debris flows have looked to connect behavior of slow moving grains with more global flow characteristics (Iverson et al., 2010; Pouliquen and Forterre, 2002), and the question

of entrainment processes continues to be relevant to industrial and geophysical interests (Morize et al. 2017; Masteller and Finnegan 2016), the interplay between different regimes is often neglected in theoretical studies of high velocity shear flows. The physics of the different rheological phases of granular materials are quite distinct, but the velocity profiles are presumably continuous, so understanding how these different regimes affect each other is crucial to understanding the overall physics of high velocity shear flows in natural settings. Rheological laws of high velocity shear flows that ignore the laws governing underlying or adjacent low velocity granular shear flows are therefore incomplete, especially with respect to the stress gradients found in natural granular flow systems.

Using a rheometer shear cell with an accelerometer attached, we measure dilation and granular temperature over a range of shear velocities for a sample of natural angular quartz grains. We use image analysis to infer a velocity profile within the flow. Using these data, we probe the relationship between the fastest-moving inertially dominated regime and the adjacent slower-moving mobilized regime. Can the observations in the lower layers be predicted based on conditions at the boundaries with the upper layers?

The answer we show in this paper is a resounding no. Subsections of the flow in these experiments can be characterized as quasistatic at the lowest velocities near the mobilization depth, inertial at the highest few grain layers just below the rotor, and transitional in between. If the behavior of each regime was independent of the others, then we would expect the velocity with depth profile of each to be identical

regardless of driving velocity, just changing entrainment depth. In this paper, we use particle image velocimetry (PIV) to measure the velocity profiles in each regime and ultimately show that both the quasi-static and transitional subsections of the flow are sensitive to driving velocity at the top. We proceed to use measurements of the bulk dilation or compaction of the flow combined with acoustic measurements to suggest that the mechanism of the coupling is acoustic waves. Rather than relying solely on boundary conditions between the subsection regimes to predict their behavior, global interactions, like those expected from acoustic compactions, appear to be required by the data.

Methods

For these experiments we used a TA Instruments AR2000ex torsional rheometer to shear 250-350 μm angular quartz sand at nine steady state velocities while under constant pressure of 3.5 kPa. The velocities tested are logarithmically spaced from 50 rad/s up to 300 rad/s, corresponding to edge velocities of 0.5 m/s to 3 m/s respectively. The rheometer is able to measure the volume of the shear flow by how much the rotor needs to raise or lower in order to maintain a constant pressure steady state for each shear velocity (Lu & Brodsky 2007; van der Elst et al. 2012).

We measured acoustic output of the flow using a Bruel and Kjaer 4373 charge accelerometer glued to a flat surface ground onto the outside of the cylindrical glass sample cell. With a sampling rate of 200kHz, accelerometer amplitude was recorded

in volts (A_v). Relative acoustic energy per grain was calculated according to Taylor and Brodsky (2017).

$$E_a = \frac{\left\langle A_v^2 \right\rangle}{N_s} \tag{2}$$

The square of A_v approximates acoustic wave energy and is averaged over a fixed time window before being normalized by N, the number of grains in the fastest moving layer of the flow closest to the recording accelerometer.

The experiment was recorded in 60 frame per second HD video using a Sony HDR-CX405 camera. After the experiment, the videos were analyzed to find the velocity profiles below the surface of the flow in the resolvable range of inertial numbers between $10^{-6} – 10^{-3}$, corresponding to linear velocities of about 10^{-5} m/s $–10^{-2}$ m/s for individual grains. Velocity analysis was done using PIVLab (Thielicke and Stamhuis, 2014).

On the same apparatus but without video data, we also conducted experiments applying an external vibration via a transducer as a sample was sheared very slowly. In this way we were able to measure friction, compaction and recovery in the presence and absence of two amplitudes of applied vibration for a range of grain sizes. Appendix B Section 1 contains procedure details and comprehensive results from these experiments.

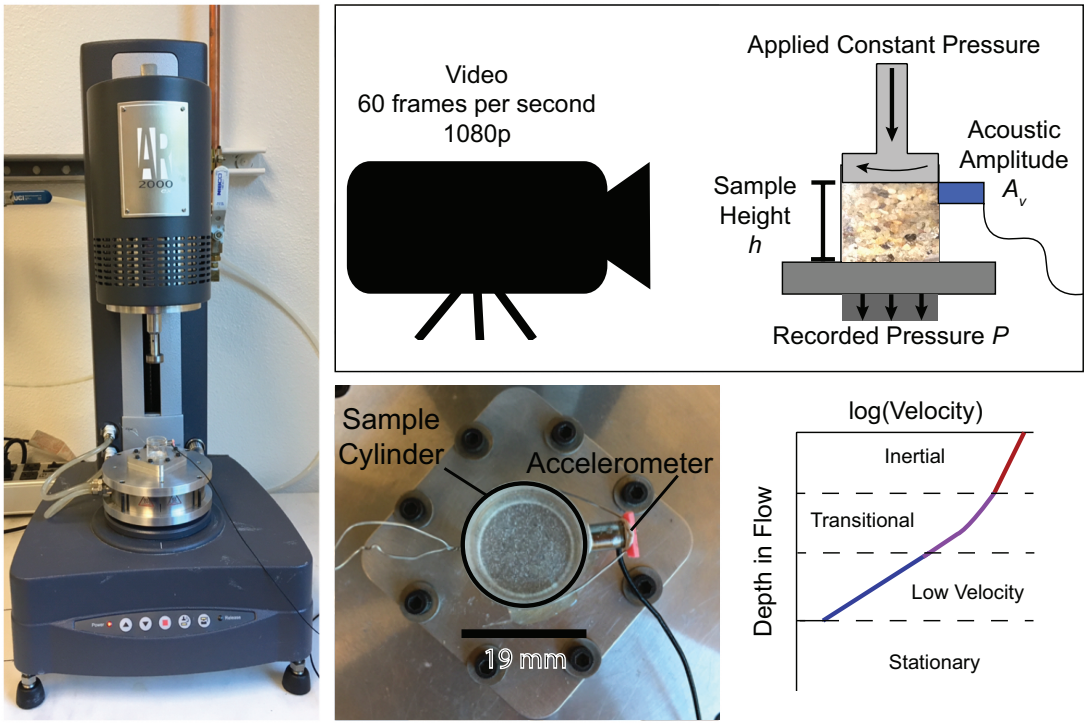

Figure 1. Photographs of rheometer and experimental set up. (left) TA Instruments AR2000ex torsional rheometer with custom rotor and sample cylinder attached. (top right) Schematic of experimental configuration showing variables that were measured. Separate video camera on tripod away from rheometer base captures images at 60 frames per second and with 1/60 second shutter speed. Images are captured with resolution of 19μm per pixel. (bottom center) Sample cylinder has a Bruel & Kjaer charge accelerometer glued to the outside of the glass at the shear zone level. (bottom right) Schematic velocity profile showing different subsections of the flow. Low velocity or quasi-static flow in blue, transitional regime flow in purple, and inertial regime flow in red.

Results

The experimental set up allowed us to measure the composite behavior of the shear flow as well as the separate behaviors of the lowest and highest velocity subsections of the flow. We discuss each of these separately below and then consider their interactions.

Composite Flow

The change in rotor height with shear velocity gives the relationship between total dilation of the flow and driving inertial number. Total dilation for these experiments scales with inertial number raised to a power of 0.9 ± 0.1. Video analysis shows that as the velocity at the top of the flow increases, the base of the flow lowers, so the total shear zone is expanding on two fronts. Lowering of the base of shear in this case is a result of entrainment of lower layers of grains as a result of the increased shear velocity, as shown in Appendix B Section 2.

Low Velocity Subsection

Along with the change in mobilization depth, we also observe differences in the velocity profiles in the slowest moving subsection of the flow. Figure 2 shows velocity profiles from the top of flow for each driving velocity tested. We examined exponential functions of the form:

$$I = Ae^{\frac{-z}{Nd}} \tag{3}$$

where I is local inertial number, A is a constant, z is depth in the flow, d is median grain diameter and N is characteristic number of grains over which velocity changes. Figure 3 shows changes in N for different driving inertial numbers in both the slow moving and fast moving subsection. In the slow moving subsection of the flow, N varies with driving inertial number raised to a power of 0.05. This means that as driving velocity increases, the difference in velocity between grain layers in the

slowest part of the flow decreases. In other words, even 10+ grain layers down, it is easier to mobilize underlying grains as driving velocity increases.

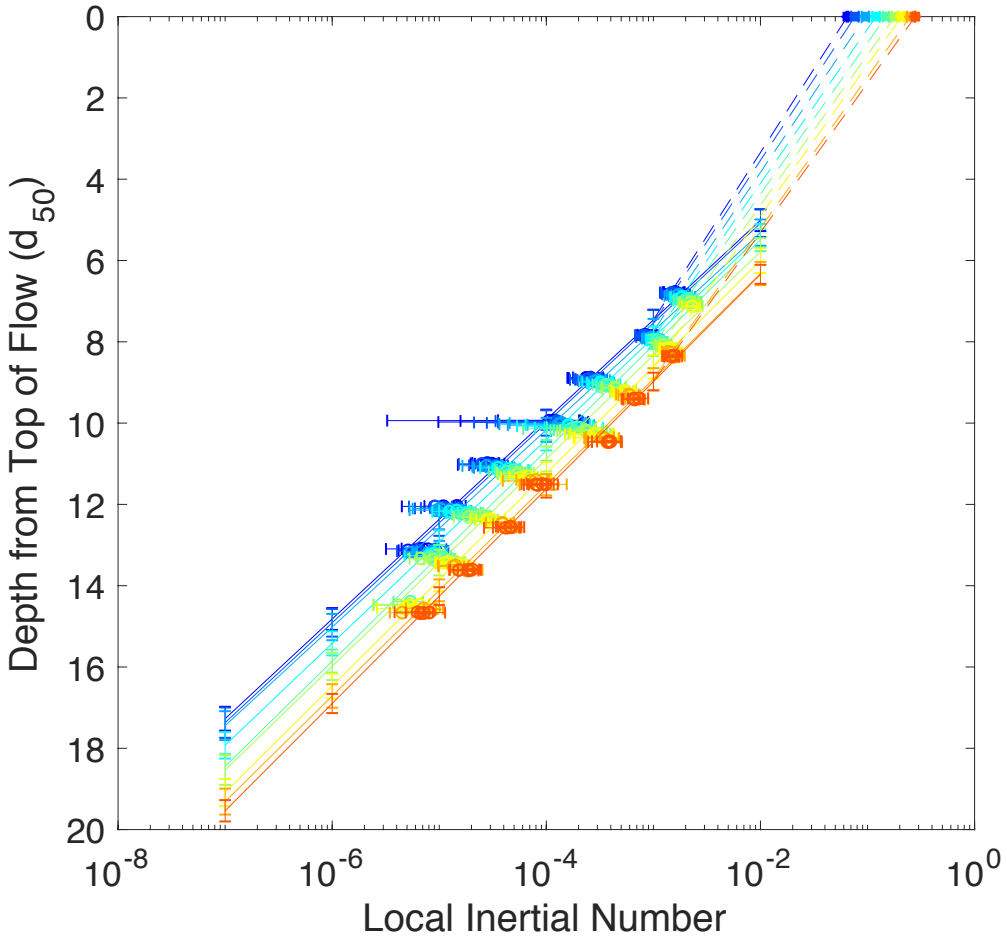

Figure 2. Velocity profiles as measured using particle image velocimetry for nine steady state driving velocities. Driving velocity is indicated by the square markers (□) at depth 0 of the flow. Local inertial number is calculated using local shear rate and depth adjusted pressure.

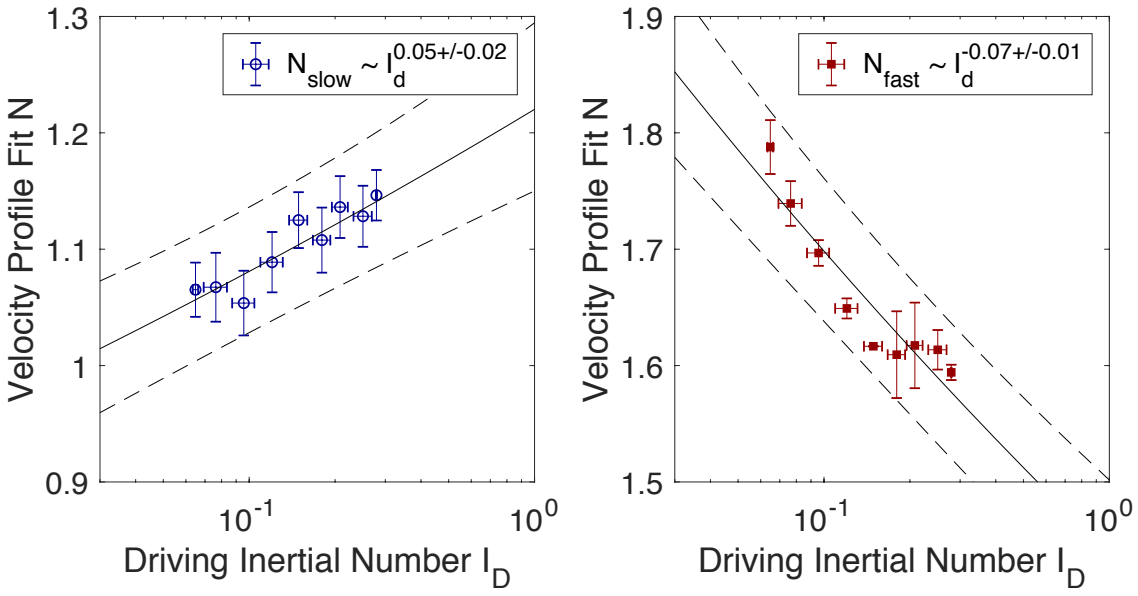

Figure 3. (left) Open circles show fit of N for low velocity profiles, and (right) filled squares show fit of N for high velocity profiles. N represents the coefficient from the equation $I=Ae^{(-z/Nd)}$ which describes the exponential velocity profile observed during shear.

Low velocity vibration experiments show that the mechanism for this change is likely a reduction in friction caused by acoustic waves. These experiments are described in detail in Appendix B Section 1. Figure 4 shows change in friction with externally applied acoustic noise amplitude for 125-500 μm diameter angular quartz grains. The value μ/μ_0 compares coefficient of friction, μ, as measured during the first 30 seconds of vibration to μ_0, the average value of coefficient of friction for the 100 seconds before vibration began. This value is plotted against recorded acoustic amplitude squared and multiplied by grain size in order to account for the difference in attenuation for different grain sizes. Applied vibration will dissipate at each grain contact. To normalize vibration energy, we would therefore wish to divide by the

number of grain diameters that span any given wave travel length L. The number of grains across such a length will be $n_L = L/d$. Therefore for any consistent length, $A^2/n_L \sim A^2 d$.

Because the limit of μ/μ_0 as A^2 approaches zero is 1 and not infinity, change in coefficient of friction with acoustic energy would be best modeled with an exponential decay function rather than a power law. In the absence of calibrated acoustic and vibration measurements, however, a power law fit suffices within the range of vibration amplitudes shown here. Coefficient of friction decreases with increasing acoustic energy raised to a power of -0.2, a finding which agrees with a similar experiment conducted using 1 mm glass beads (Dijksman et al., 2013). Combining the observations from Figure 3 and Figure 4 implies that velocity profile fit parameter, N_{slow} (eq. 3), is sensitive to friction changes following the relationship:

$$N_{slow} \sim \mu^{-\frac{1}{4}} \tag{4}$$

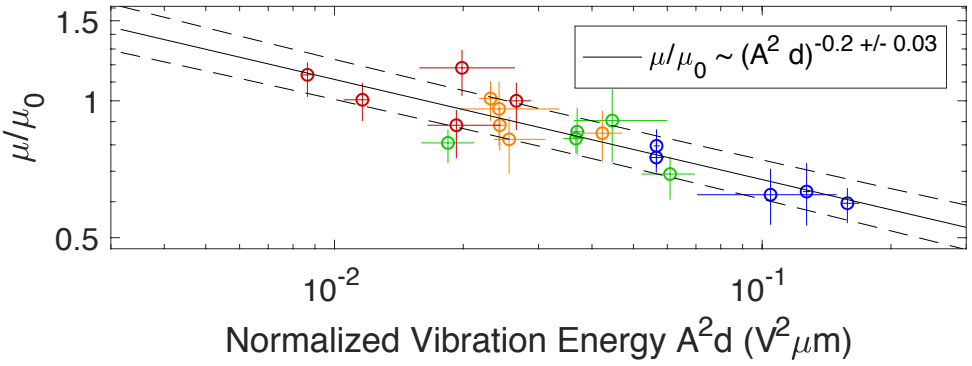

Figure 4. Externally applied vibration through a transducer resulted in reduced friction, with increasing vibration amplitude corresponding to further decreasing friction. Each point represents results from first 30 seconds of vibration for all grain sizes tested. 125-180 μm (red), 180-250 μm (orange), 250-355 μm (green), and 355-500 μm (blue).

Transitional and High Velocity Subsections

Above inertial numbers of 10^{-3}, the change in velocity profiles with driving velocity is more dramatic. As driving velocity increases, N_{fast} decreases, meaning the rate of change of velocity with depth increases such that a larger range of velocities is covered over a smaller thickness of the flow. All driving velocities tested result in inertially dominated flow regimes in the fastest parts of the flow. We assume that the physics of these collisionally controlled fastest-moving layers remains fundamentally the same and suggest that this change in the velocity profile is generated by compaction of more slowly moving grains at transitional inertial numbers between 10^{-3} to 10^{-1}.

As driving velocity increases, the noise produced by grain collisions also increases. The amplitudes of vibrations produced by grain collision are powerful enough to cause compaction of slowly sheared grains. Presumably over the course of conditioning, the slowest moving and immobilized grains in the sample have been compacted as much as is possible. The only recoverable vibration-induced compaction is therefore in these transitional shear velocities found between 10^{-3}-10^{-1} inertial numbers. Above inertial numbers of about 10^{-1}, flows enter more definitively into the inertially dominated regime, so grains moving at or above these speeds should not experience compaction as the result of exposure to vibration. This is consistent with results from previous experiments (van der Elst et al. 2012) as well as our new results testing the response of slowly sheared granular media to externally applied vibration.

The grain layers moving at these velocities are weakened and compacted during flow in the presence of higher amplitude acoustic waves produced by grain-grain collisions at the higher shear velocities, but this effect is removed in the absence of this noise, and these layers become stronger and dilate when the driving velocity and thus the noise of the flow is reduced.

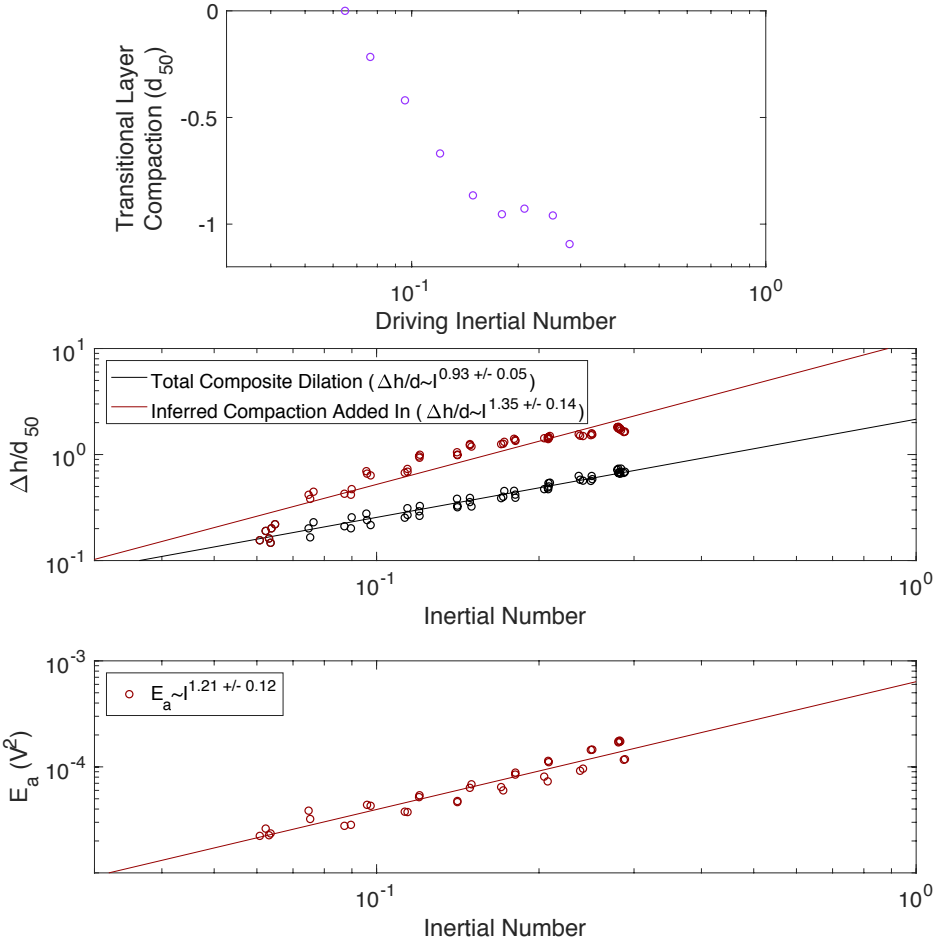

Figure 5. (top) Assuming a consistent high velocity layer profile, transitional velocity layers would have to thin with increasing driving velocity. (middle) Black markers show dilation as measured by change in rotor height only. Red markers show change in rotor height combined with change in base of flow to give a measurement of total dilation of the shear zone with driving inertial number. (bottom) Red markers show linear relationship of acoustic energy with driving inertial number of the flow.

Assuming that the velocity profile of the fastest moving grain layers is similar for all driving velocities, the amount of compaction in the slow-to-transitional velocity layers can be estimated by observing the difference in between the thickness of this layer for each steady state velocity if the fastest moving velocities all have the same general profile above inertial numbers of 10^{-1}. When the amount of compaction in these layers is added into the overall dilation measurement of the flow, we observe that flow dilation is actually linear with granular temperature and driving velocity of the flow (Figure 5). This is consistent with existing theory.

To verify the cause of this inferred compaction, we compared the relationship between compaction and acoustic energy for this experiment with the relationship observed for two separate experiments. In van der Elst et al. (2012), compaction was observed as a result of shear-induced acoustic noise over a range of velocities in the transitional flow regime, between inertial numbers of 10^{-3} – 10^{-1}. We separately conducted experiments applying external vibrations to very slowly shearing, i.e. quasistatic regime, angular quartz grains of various sizes. To compare these three experiments, the amount of compaction measured in each was normalized by the number of grain layers in the flow between a mobilization inertial number of $I = 10^{-6}$ and the limit of truly inertial flow where $I = 10^{-1}$. Figure 6 shows the compaction resulting from increasing vibration strength, with acoustic energy normalized by grain diameter, which describes the difference in penetration depth of the vibrational noise for different grain sizes tested.

As driving velocity increases, there is a subtle flattening of both N_{fast} (Figure 3) and the inferred transitional layer compaction (Figure 5). This implies that there is a maximum amount of compaction by vibration in these shear layers, beyond which increases in acoustic wave energy will not continue to compact. Figure 6 implies that this flattening occurs near 10% total compaction. This compaction amount approximates the difference between the values generally considered as the random loose packing fraction Φ=0.54 and random close packing fraction Φ=0.64 (Silbert 2010; Jerkins et al. 2008; Onoda and Liniger 1990) for static grain packs, and thus it is reasonable that this would be near the limit of potential compaction amounts.

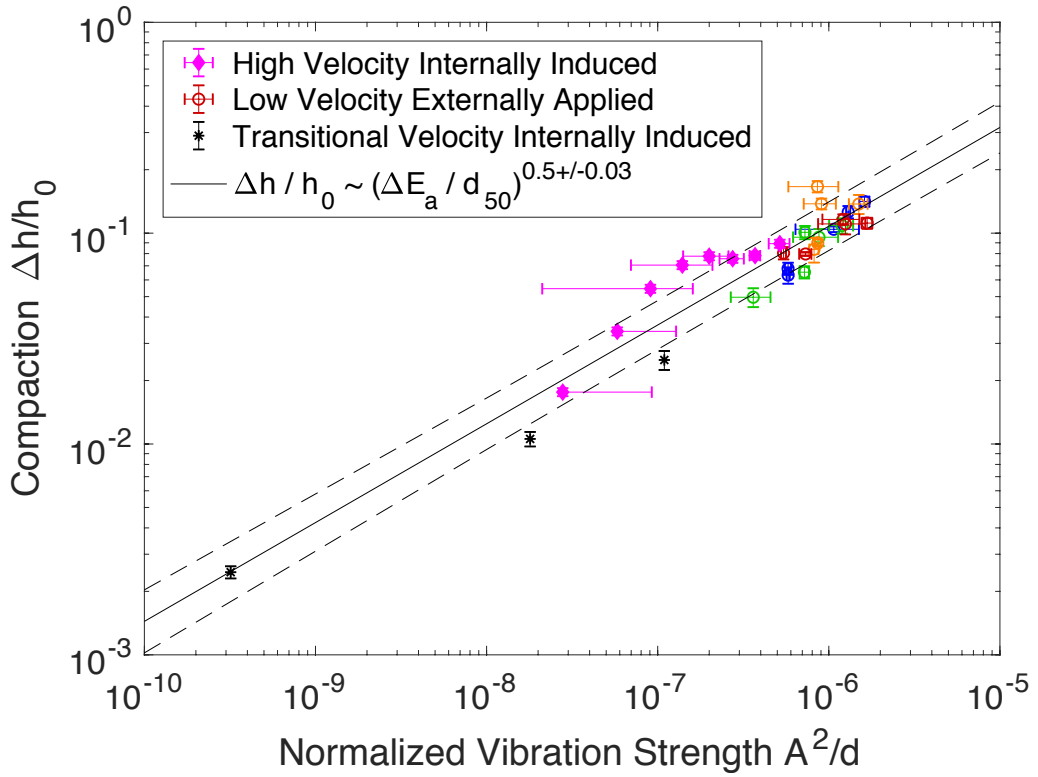

Figure 6. Compaction as a fraction of original low velocity shear zone height is a function of the square root of vibrational noise energy normalized by grain size. This scaling holds true for cases where acoustic energy is internally induced during shear at either low or high velocities and also for cases where acoustic energy is externally applied as a vibration during low velocity shear.

Regardless of flow regime or source of acoustic noise, we find that compaction scales with square root of vibration strength, implying that the same mechanisms observed in the lower velocity experiments are operating in the interior of the high velocity flow. This shows that the high velocity flow is not operating with wholly separate physics than the lower and transitional velocity flows, and in fact the effect of the fastest moving grains on the rheology and susceptibilities of these regimes must be considered when formulating a global understanding of a dense granular shear flow.

Interpretation

The implications of this finding are straightforward. It is no longer sufficient to study granular flow rheology as a set of separate regimes. In most natural or industrial settings, where there is a high velocity flow there is necessarily interaction between that high velocity flow and the abutting low velocity flow sections that complete the continuous velocity profile of the flowing granular media.

These types of interactions have been examined through the lens of fluidity literature (Henann and Kamrin 2013; Kamrin and Koval 2012), which attempts to quantify nonlocal effects in a dense flow regime in terms of grain communication length scales. Preliminary comparison of our data with a nonlocal fluidity model shows differences between these types of models, which were developed with spherical particles in mind, and the behavior of more naturally varied grains. Figure 7

shows velocity profiles as measured in these experiments and as predicted by nonlocal fluidity model from the Henann Group at Brown University. Normalized angular shear velocity, $\hat{\Omega}$, is a slight modification of inertial number and defined as

$$\hat{\Omega} = \omega_0 d \sqrt{\frac{\rho}{P}} \tag{4}$$

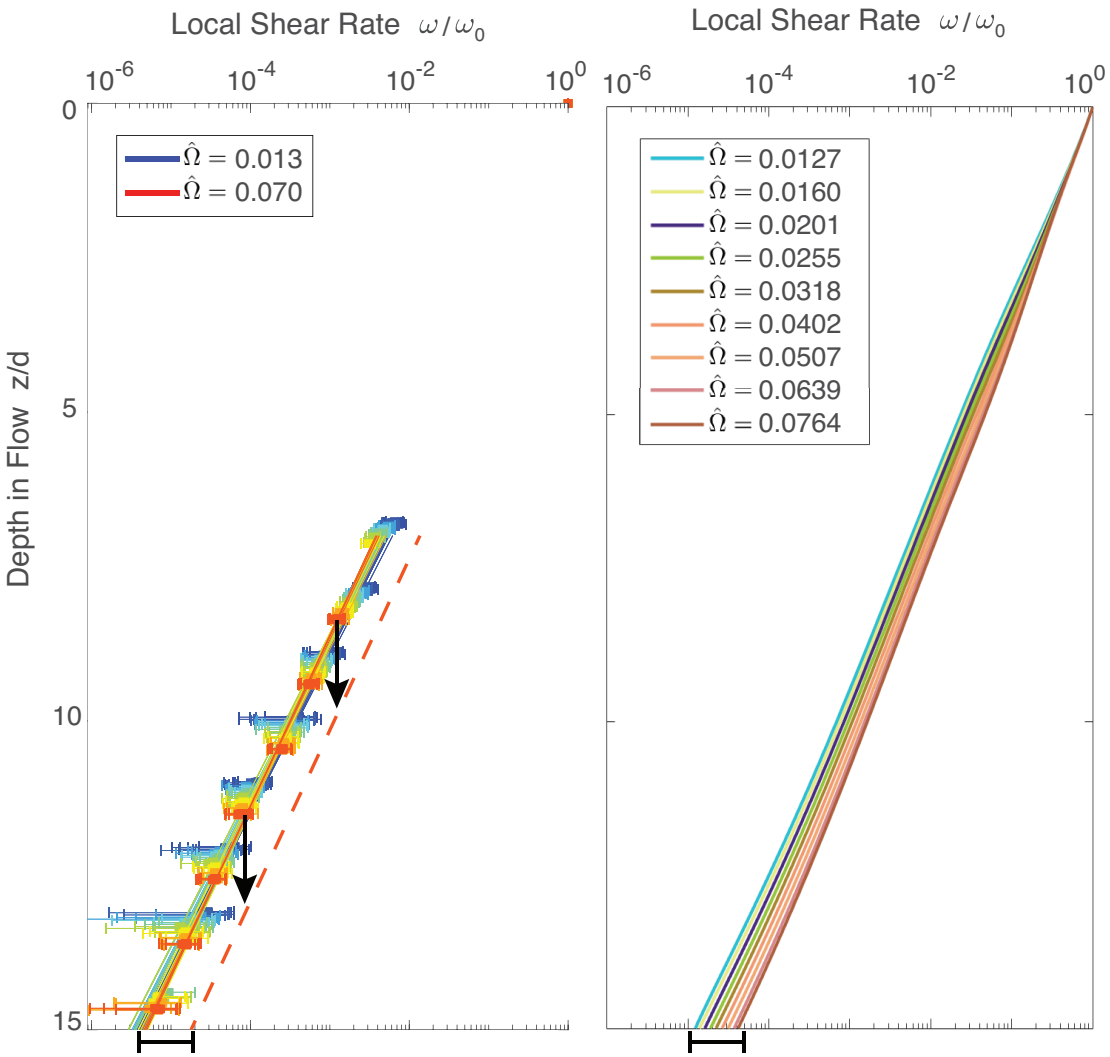

Figure 7. (left) Velocity profiles from angular quartz experiments, colors coded to shear velocity in the same way as Figure 2. (right) Predicted velocity profiles from nonlocal granular flow rheology FEM. $\hat{\Omega}$ is normalized shear rate, ω/ω0 is fraction of driving angular velocity observed at depth in the flow, z/d. Dashed red line shows approximate depth of flow profile as predicted by FEM.

The nonlocal fluidity model predicts that as driving velocity increases, faster flow will diffuse deeper into the grain pack. While the change in slope of the lower velocity portion of the experimentally observed velocity profiles is consistent with the change in slope predicted by nonlocal rheology FEM, the absolute depth change does not. The approximate difference in depth of flow between experiments and model for the fastest driving velocities tested is shown by the black arrows separating the solid red line (experimental data) from the dashed red line (approximate model depth). This could be explained by the suggested transitional velocity layer weakening. Experimental data most likely deviates from the model at velocities higher than those for which experimentally measured velocity profiles are available. If the layer of grains moving at transitional regime velocities is thinner than that predicted by the nonlocal rheology model, that could explain the difference in flow depth between the experiments and the nonlocal fluidity model.

Conclusions

Rather than observe separate regimes of granular flow operating independently of one another, we observe that (a) the profile of the slowest quasi-static regime of flow steepens with increasing driving velocity, indicating a reduction of friction and increased entrainment and (b) the transitional and inertial regimes show a shallowing of velocity profile with increasing driving velocity, indicating

compaction and weakening in the transitional subsection of the flow as a result of the vibration produced by flow noise.

Inertially controlled grain collisions are what drives dilation at high velocity flows, but the noise and acoustic waves produced by these impacts have the same effect on the slower parts of the flow that any applied vibration would have. Thus low and transitional inertial number sections of the flow will have a different response to different driving velocities precisely because of the different amplitude vibrations that such flows produce.

References

Brilliantov, N. V., & Pöschel, T. (2004). Kinetic Theory of Granular Gases. Oxford: Oxford University Press.

Cody, G. D., Goldfarb, D. J., Storch, G. V., & Norris, A. N. (1996). Particle granular temperature in gas fluidized beds. *Powder Technology*.

da Cruz, F., Emam, S., Prochnow, M., Roux, J.-N., & Chevoir, F. (2005). Rheophysics of dense granular materials: Discrete simulation of plane shear flows. *Physical Review E*, *72*(2), 341. http://doi.org/10.1016/0032-5910(81)87039-8

Dijksman, J. A., Wortel, G. H., van Dellen, L. T. H., Dauchot, O., & van Hecke, M. (2011). Jamming, Yielding, and Rheology of Weakly Vibrated Granular Media. *Physical Review Letters*, *107*(10), 108303. http://doi.org/10.1103/PhysRevLett.107.108303

Henann, D. L., Kamrin K. (2013). A predictive, size-dependent continuum model for dense granular flows. *Proceedings of the National Academy of Sciences, 110*, 6730–6735. DOI: 10.1073/pnas.1219153110

Iverson, R. M., Reid, M. E., Logan, M., LaHusen, R. G., Godt, J. W., Griswold, J. P. (2010). Positive feedback and momentum growth during debris flow entrainment of wet bed sediment. *Nature Geoscience, 4,* 116-121.

Jaeger, H. M., Liu, Chu-heng and Nagel, S. R. (1989). Relaxation at the Angle of Repose. *Phys. Rev. Lett.* 62, 40.

Jaeger, H. M., Nagel, S. R., & Behringer, R. P. (1996). Granular solids, liquids, and gases. *Reviews of Modern Physics*, *68*(4), 1259–1273.

Jerkins, M., Schr¨oter, M., Swinney, H. L., Senden, T. J., Saadatfar, M. and Aste, T. (2008). Onset of mechanical stability in random packings of frictional spheres. *Phys. Rev. Lett.*, *101*, 018301.

Kamrin K, Koval G. (2012). Nonlocal Constitutive Relation for Steady Granular Flow. *Physical Review Letters, 108*, 178301–6. DOI: 10.1103/PhysRevLett.108.178301

Lu, K., Brodsky, E. E., & Kavehpour, H. P. (2007). Shear-weakening of the transitional regime for granular flow. *Journal of Fluid Mechanics*, *587*.

http://doi.org/10.1017/S0022112007007331

Masteller, C. and Finnegan, N. (2016). Interplay between grain protrusion and sediment entrainment in an experimental flume. *Journal of Geophysical Research - Earth Surface, 122(1),* 274-289.

Morize, C., Herbert, E., & Sauret, A. (2017). Resuspension threshold of a granular bed by localized heating. *Physical Review E 96(3)*, 032903.

Ogawa, S. (1978). Multitemperature theory of granular materials. (S. C. Cowin & S. M, Eds.). Tokyo: Gakujutsu Bunker Fukyukai.

Onoda, G. Y. and Liniger, E. G. (1990). Random loose packings of uniform spheres and the dilatancy onset. *Physical Review Letters, 64,* 2727.

Pouliquen, O., & Forterre, Y. (2002). Friction law for dense granular flows: application to the motion of a mass down a rough inclined plane. *Journal of Fluid Mechanics*, *453*. http://doi.org/10.1017/S0022112001006796

Silbert, L. E. (2010) Jamming of frictional spheres and random loose packing. *Soft Matter, 6,* 2918-2924.

Taylor, S. and Brodsky, E.E. (2017). Granular temperature measured experimentally in a shear flow by acoustic energy. *Physical Review E, 96,* 032913.

Thielicke, W. and Stamhuis, E.J. (2014) PIVlab – Towards user-friendly, affordable and accurate digital particle image velocimetry in MATLAB. *Journal of Open Research Software* 2(1):e30, DOI: http://dx.doi.org/10.5334/jors.bl

van der Elst, N. J., Brodsky, E. E., Le Bas, P.-Y., & Johnson, P. A. (2012). Auto-acoustic compaction in steady shear flows: Experimental evidence for suppression of shear dilatancy by internal acoustic vibration. *Journal of Geophysical Research*, *117*(B9), B09314. http://doi.org/10.1029/2011JB008897

Warr, S., Huntley, J. M., & Jacques, G. (1995). Fluidization of a two-dimensional granular system: Experimental study and scaling behavior. *Physical Review E*.

Chapter 3

Energy partitioning in granular flow depends on nano scale plastic work

Introduction

Understanding the basic physics of flowing granular materials has proved elusive for experimentalists, theorists and modelers alike. Constitutive laws predicting a granular material's resistance to stress require taking into account both complex inter-granular structures as well as variable sources of energy dissipation. Examples of dissipative energy sinks include velocity fluctuations, grain rotations, deformation of force networks, grain fracture, plastic deformation of grains, and frictional heat.

The relative magnitude of these potential sinks can be parsed by considering how different grain properties contribute to different types of energy dissipation. Grains with different strengths, shapes and elastic moduli will crush, rearrange, or bounce around differently. In high velocity granular flows, a great deal of input energy is lost in the form of velocity fluctuations, represented by the average amount that an an individual grain's instantaneous velocity varies from the average velocity of the flow. As flow velocity increases, fluctuation energy also increases. This

fluctuation energy is known as granular temperature in analogy to kinetic theories of molecular gases. Granular temperature can, as in the ideal gas law, contribute to a strengthening or expansion of a high velocity granular flow, but some portion of this granular temperature is dissipated in the flow in other ways. Chapter 2 showed that dissipation of granular temperature can take the form of grain rearrangements in slower parts of the shear zone that can have a significant effect on the overall rheology of a flow. Accurate prediction of shear flows of granular materials with different shapes and compositions requires an understanding of how these properties affect energy dissipation in the flow.

Coefficient of restitution has long been considered important to the energy balance of granular flows (Campbell, 2006; Haff, 1983; Jenkins & Savage, 1983). Coefficient of restitution is carefully measured through the collision of spheres of identical composition, however it is also frequently approximated mathematically as scaling with the square root of the ratio of indentation hardness over elastic modulus (Andreotti et al., 2013; Johnson 1985). For nonspherical grains, however, this approximation is incomplete, as asphericity can partition a particle's rebound energy into a combination of translational and rotational energy (Glielmo et al. 2014). Even slight asphericities can alter the distributions of coefficient of resitution measurements. As grains become more irregularly shaped this effect becomes even more pronounced, and within a range of relatively hard materials sheared at high velocity, it is reasonable to assume that angular or non-spherical shape will have more

of an influence on flow rheology than the idealized coefficient of restitution for the given material.

Granular flows of high societal importance are those involving geologic processes and materials, where hazard assessment and engineering solutions require proper modeling of granular flow stress response for grains of different composition, shape, size, roughness and angularity. Transport and use of granular materials in construction and pharmaceutical industries similarly relies on understanding how grain properties will affect the rheologic response of the aggregate flow. Different naturally occurring minerals can exhibit quite different elastic moduli and plastic deformation behavior, and there are different ways to quantify this.

The strategy of this study is to start with an array of material properties related to the bulk rheology of the materials being tested. Since the primary deformation regimes are plastic, elastic and fracture, we chose hardness, Young's modulus and fracture toughness as representative parameters. Our goal is to determine what combination of these parameters provides the best prediction of the observed flow behavior. After a brief review of these parameters and their role in determining the failure regime, we describe the experiments. Five mineral sands chosen from the list of characteristic minerals on the Mohs hardness scale were sheared at high velocities under constant pressure while measuring dilation and acoustic energy produced by the flow. We compare how dilation and acoustic energy scale with shear velocity. The separation of these scalings suggests energy partioning in the flow, as explored in

Chapter 2. We find that plastic displacement length best predicts differences in energy partitioning between different mineral sands.

Quantifying plasticity and brittleness

A material's hardness, fracture toughness and elastic moduli combine to describe its failure criteria. We review the definitions and measurement methods for hardness, fracture toughness and Young's modulus and explore how these properties combine to predict different aspects of fracture and failure.

Hardness in materials science is a quality that broadly describes resistance to permanent deformation, and different evaluation techniques measure this in different ways. Hardness is thought of as a proxy for yield strength, and Vickers hardness, *H*, is a measurement of how much force is required per area of deformation caused by a square pyramid tipped indenter (Hertz 1896; Tabor 1951, 1970; Lawn et al. 1980; Broz et al 2006):

$$H = \frac{F}{2a^2} \tag{1}$$

This deformation is considered plastic and is measured based on the area of the unrecovered dent left in the material after the indentor is removed. The force applied is represented by *F,* and *a* is the length of plastic deformation. It is important to note that Vickers hardness scales with yield strength, but it is a test-dependent quantity and not a material property in the strictest sense. Furthermore, this definition of hardness is distinct from the mineralogical definition of Mohs hardness, which measures

scraching. The two quantities are related, but the Mohs scale is an index based on relative measures whereas Vickers hardness is measured in physical units of stress that are more readily utilized for interpreting process.

Fracture toughness is an experimentally measured quantity that describes the critical stress intensity needed to propagate an existing crack:

$$K_C = \psi \sigma c^{1/2} \tag{2}$$

where ψ is a geometry factor, σ is applied stress and c is crack length (Lawn, 1993).

An elastic modulus in general is a ratio of stress over the reversible strain resulting from the applied stress. Young's modulus in particular, E, describes the ratio of applied stress over the change in length of an object resulting from that strain:

$$E = \frac{F / A}{\Delta L / L} \tag{3}$$

where F/A is the applied stress, ΔL is the resulting change in length, and L is the original length of the object (Young, 1845).

These parameters can describe a material's energetic response to stress. A grain under pressure can respond elastically, plastically or through fracture. Previously relative plastic and fracture damage has been described using a ratio of hardness over fracture toughness, known as the brittleness index (Lawn & Marshall, 1979):

$$B = \frac{H}{K_C} \tag{4}$$

Rather than compare relative amounts of damage, for a granular system the more relevant comparison is energy partitioning between plastic damage and fracture

energy. The critical energy release rate required for fracture propagation can be represented by

$$G_C = R_0 = \frac{K_C^2}{E} \tag{5}$$

for an unconfined grain, where K_C is fracture toughness and E is Young's modulus (Griffith, 1921; Lawn 1993; Akono et al. 2011). Per crack surface area, the crack resistance energy, R_0, is equal to the fracture energy release rate, G_C, for a brittle material. In equilibrium, fracture energy release, G, is equal to crack resistance energy, R. Crack resistance energy describes dissipation in the material and represents the sum of both the surface energy of the solid as well as a plastic work term, R_P (Irwin, 1958; Orowan, 1955).

To take into account energy dissipation in the form of plastic work, we consider the cohesion zone model (Barenblatt, 1962), which suggests a small zone of plastic deformation near the crack tip, the size of which does not depend on the length of the crack but rather on properties of the material. With two simplifications, plastic displacement, δ, can be estimated.

$$\delta = \frac{K_C^2}{E H} \tag{6}$$

The first simplification relies on the assumption that cohesive stress in a solid can be approximated by a hardness measurement. This seems a fair assumption because hardness seeks to measure the stress at which permanent deformation occurs and thus the stress at which cohesion is overpowered. The second simplification then requires that cohesive stress does not vary over the length of the cohesion zone and can be

represented by a mean value. The true function of cohesive stress within the cohesion zone is more complicated, but analytically the mean serves as a valuable approximation (Lawn, 1993).

Plastic displacement, δ, can be thought of as the amount of displacement that will occur before a crack will propagate through and fracture a grain, and it should also be thought of as the amount of plastic displacement that accompanies any crack formation. Combined with average contact forces between grains, δ can efficiently represent the amount of energy dissipated in the form of plastic work. Where δ is high, grains will dissipate more energy in the form of plastic deformation, and where δ is low, grains are more prone to forming cracks and fractures, and dissipate less energy in the form of plastic damage. For the experiments presented here, grains are of similar grain size and shape and all subjected to the same constant normal pressure, thus contact forces between grains are similar.

The dependence of dissipative behavior in a granular flow on material properties of grains has until now been considered mostly in terms of coefficient of restitution, but the field has lacked experiments covering a range of velocities and material properties, especially in irregularly shaped grains. With this study, we look to clarify how different grain material properties change how a high velocity flow will dissipate fluctuation energy. As grains move faster and collisions create more elastic wave energy and near-neighbor perturbations, the bulk behavior of the flow will depend on how this energy diffuses into slower moving layers and what effect it has.

We will specifically examine how effective H, K_C, E, brittleness index B, fracture energy release rate G_C, and plastic displacement δ, as predictors of dilatant behavior.

Methods

Using the experimental set up and methods of Taylor & Brodsky (2017), we measured dilation and acoustic energy while shearing different mineral sands at nine steady state velocities while under constant pressure of 3.5 kPa. Samples were sheared using a TA Instruments AR2000ex torsional rheometer (Figure 1) with a cylindrical sample cell with sample grains glued to both the bottom of the shear cell and the surface of the disk rotor. An accelerometer glued to the outside of the shear cell recorded acoustic energy produced by colliding grains in the shear zone. Velocities tested ran between 50 rad/s through 300 rad/s, which corresponds to linear velocities along the outer circumference of 0.5 – 3 m/s.

The Mohs hardness scale is a well known qualitative scale to describe mineral scratch resistance. Its characteristic minerals, talc, gypsum, calcite, fluorite, apatite, orthoclase, quartz, topaz, corundum, and diamond, represent ordinal Mohs values of one through ten, respectively. Because of the abundance of these characteristic minerals and the historic use of the Mohs hardness scale in geology, there are a number of existing studies measuring different material properties of these minerals. By using Mohs characteristic minerals, we were able to draw on these exisiting studies to compare the relative influence of different material properties on

dissipation and overall flow rheology. We avoided Mohs values below four, as these mineral sands tended to exhibit a high degree of grain breakage under shear. Furthermore, diamond proved too strong for the glass sample cylinder and steel rotor. With available samples of charactersitc Mohs hardness minerals between hardnesses of three and ten, we tested granular samples of fluorite, apatite, orthoclase, quartz and corundum.

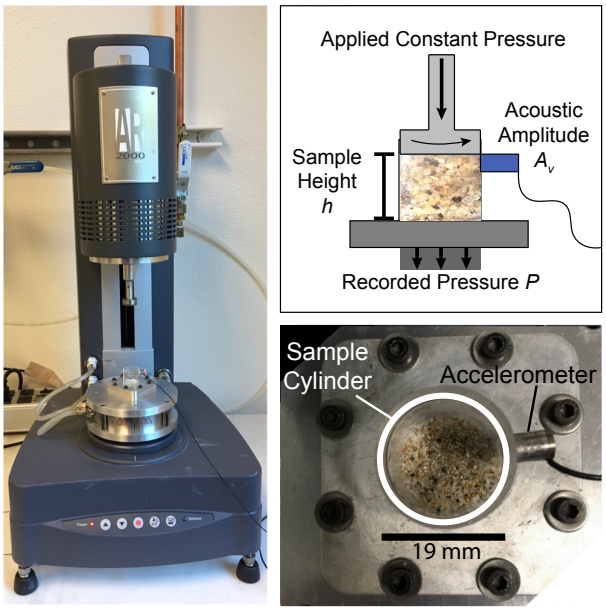

Figure 1: Photographs of rheometer and experimental set up. (left) TA Instruments AR2000ex torsional rheometer with custom rotor and sample cylinder attached. (top right) Schematic of experimental configuration showing variables that were measured. (bottom right) Sample cylinder has a Bruel & Kjaer charge accelerometer glued to the outside of the glass at the shear zone level.

Acoustic energy, E_a, is calculated after (Taylor & Brodsky, 2017) as the square of accelerometer amplitude, A_V, divided by the number of outermost grains in the fastest moving layer, N_S.

$$E_a = \frac{\langle A_V^2 \rangle}{N_S} \tag{7}$$

To compare the acoustic energy between mineral samples, we normalize E_a by grain mass, m_{gr}.

Samples were prepared by crushing mineral hand samples, collecting beach sand or ordering industrial grit samples. Table 1 shows material properties as well as preparation technique for each sample tested.

Table 1

Sample	ρ (kg/ m^3)	Vickers Hardness* (GPa)	Fracture toughness* (MPa $m^{1/2}$)	Elastic Modulus* (GPa)	Aspect Ratio	Grain Size (mm)	Source
Fluorite	2870	2.00 ± 0.10	0.89 ± 0.13	139.7 ± 3.8	1.8 ± 0.9	0.25-0.36	Crushed
Apatite	2670	5.43 ± 0.33	0.76 ± 0.13	150.8 ± 6.4	1.8 ± 0.6	0.25-0.36	Crushed
Orthoclase	2110	6.87 ± 0.66	0.88 ± 0.13	89.2 ± 7.1	-	0.25-0.36	Crushed
Quartz	2530	12.2 ± 0.60	1.60 ± 0.16	117.6 ± 2.7	1.4 ± 0.3	0.25-0.36	Beach
Corundum	3480	19.6 ± 0.5	2.38 ± 0.22	376.1 ± 9.8	1.8 ± 0.5	0.33	Industrial

** From Broz et al. 2006*

Hardness, fracture toughness and elastic modulus were measured using depth-sensing indentation experiments (Broz et al., 2006).

Results

Behavior varies slightly with different grains. Figure 2 shows the change in sample height and acoustic energy for each mineral at each velocity tested. Minerals are plotted separately in order to avoid comparing starting points for the sample height measurements, and to make it easier to observe differences in the shape and

range of the data sets. Fluorite dilates the most with velocity of all samples tested and produces the least acoustic energy. The subtle differences in how dilation and acoustic energy vary with shear rate are best compared as differentials. Figure 3 shows that dh/dE_a changes with inertial number for all minerals tested. The negative aspect of this relationship can be attributed to the effect described in Chapter 2. As velocity in the flow increases and noise produced by the flow increases, a greater portion of the acoustic energy gets diverted away from dilating the fastest part of flow and into performing work on slower sections of the flow. This partitioning of energy is present for all minerals tested, however the amount varies with mineral properties.

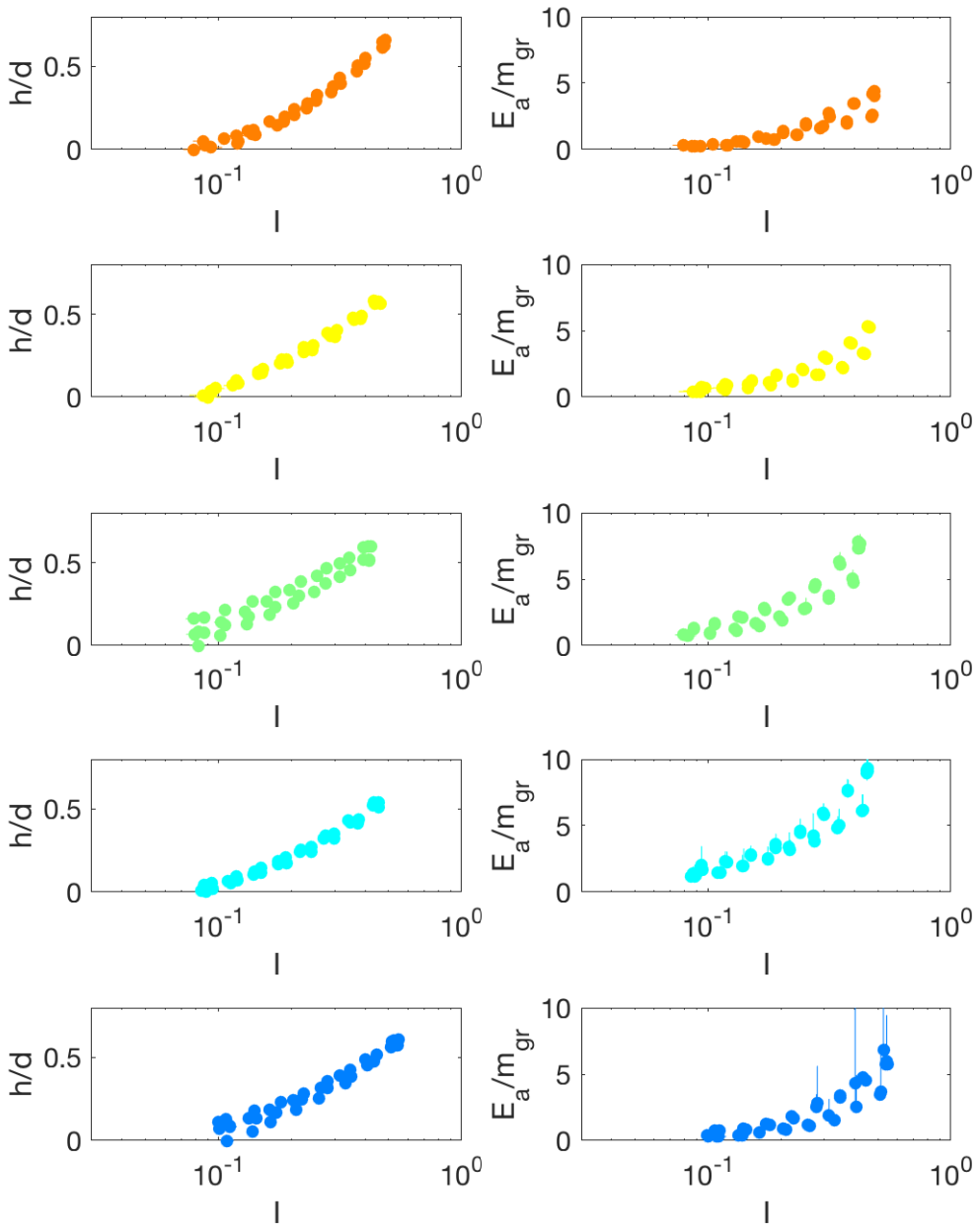

Figure 2. (left) Height of sample normalized by grain diameter and (right) acoustic energy for minerals tested. From top: fluorite (orange), apatite (yellow), orthoclase (green), quartz (cyan), and corundum (blue).

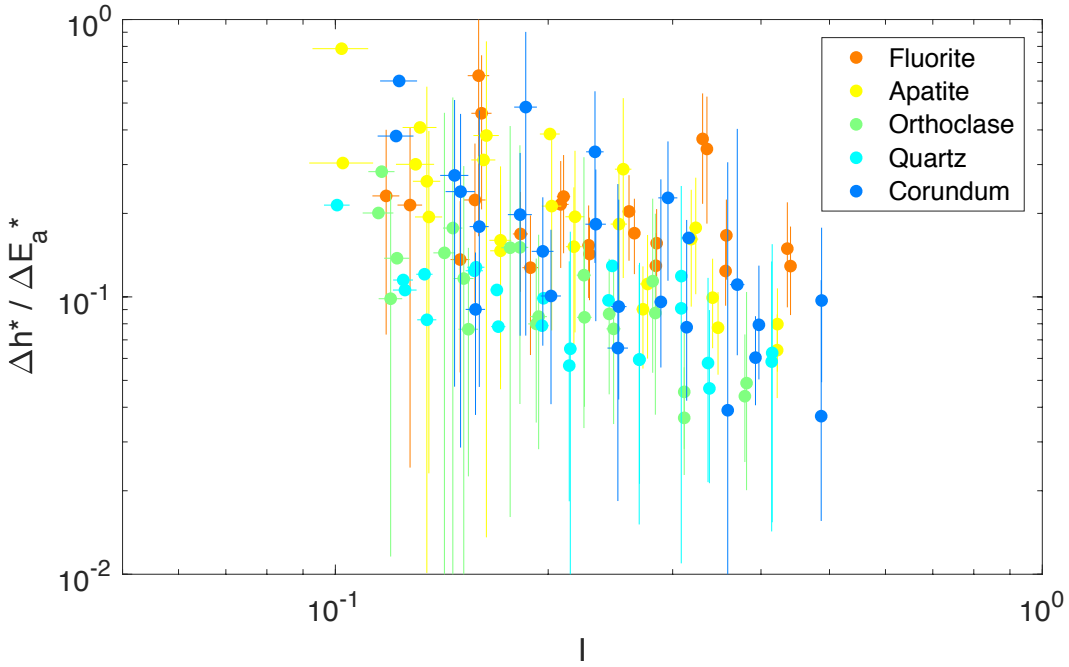

Figure 3. Change in sample height normalized by median grain diameter divided by change in acoustic energy between two velocity steps for all velocities tested. $\Delta h^* = \Delta h/d$, and $\Delta E_a^* = \Delta E_a/m_{gr}$

In Figures 3 and 4, Δh^* is change in height normalized by grain diameter, $\Delta h/d$, and ΔE_a^* is change in acoustic energy normalized by grain mass, $\Delta E_a/m_{gr}$ Fluorite, the weakest mineral tested, exhibited the least amount of change in dilation noise dependence with shear velocity, while corundum, the strongest mineral tested, shows the strongest negative relationship with shear velocity. We fit a power law to find the exponent, X, describing how dilation's dependence on acoustic energy varies with inertial number for each mineral tested. Figure 4 shows how X varies with different material characteristics: Vickers hardness, H *(eq. 1)*, Young's modulus, E *(eq. 3)*, fracture toughness, K_C (*eq. 2)*, brittleness, B *(eq. 5)*, fracture energy release rate, G_C *(eq. 4)*, and plastic displacement, δ *(eq. 6)*.

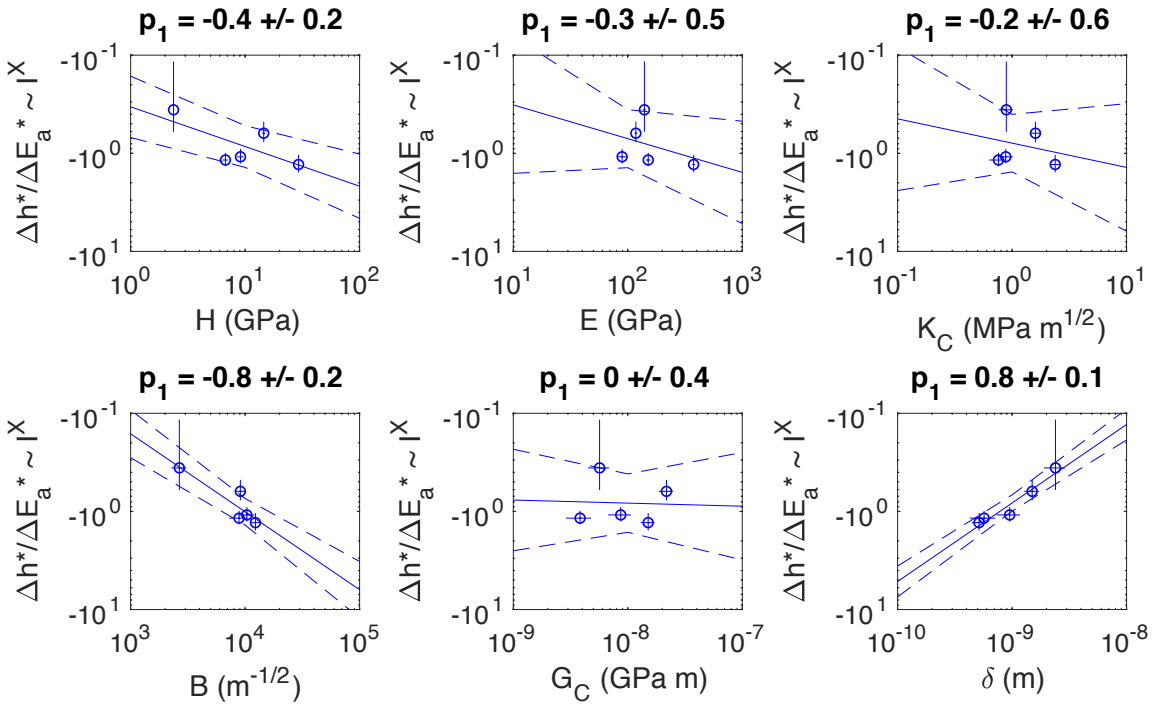

Figure 4. Variation of X with (top left) Vickers hardness, (top center) Young's modulus, (bottom left) brittleness, (bottom center) fracture energy release rate, and (bottom right) plastic displacement. $\Delta h^* = \Delta h/d$, and $\Delta E_a^* = \Delta E_a/m_{gr}$

While energy partitioning in the flow, *X,* varies for different grains, aspect ratio does not, so the influence of aspect ratio cannot be evaluated with these experiments. There is demonstrably no relationship between energy partitioning and elastic modulus, fracture energy release rate or fracture toughness. There is some evidence for a relationship with grain hardness and brittleness index. The best predictor of *X*, however, is plastic displacement, δ. When this length is high, it indicates higher susceptibility of surface damage in the form of plastic strain. When it is low, this indicates less loss of energy to surface damage and higher likelihood of fracture. For all minerals tested, grain breakage was minimal. Appendix C shows grain breakage measurements for quartz and fluorite.

Interpretation

As suggested in Chapter 2, the energy partitioning in high velocity flow is similar for all angular grains regardless of material properties in that some portion of fluctuation energy in the fastest part of the flow gets diverted to rearrangement in slower parts of the flow. The negative variation of dilation's dependence on acoustic energy with shear velocity shows this. The specific slope of $\Delta h/\Delta E_a$ appears to vary most closely with the plastic displacement length. We find that $d(\Delta h/\Delta E_a)/dI$ *varies with* δ according to the relationship:

$$\frac{\log\left(\Delta h / \Delta E_a\right)}{\log\left(I\right)} \sim \delta^{0.8\pm0.1} \tag{8}$$

Representing plastic work when combined with inter grain contact forces, this value describes a material's tendency to absorb energy plastically versus release energy through fracture, creation of new surface area and radiation of elastic waves.

Plastic displacement could affect the relationship between dilation, acoustic energy and shear velocity of a granular flow through both damage-dampening of fluctuation energy and amplification of acoustic energy. Weak grains that damage more easily, absorb excess fluctuation energy into surface damage and plastic deformation, while harder grains pass on fluctuation energy to neighbor grains. This passing of energy to neighbor grains facilitates grain rearrangements in slower parts of the flow that ultimately change the composite rheology. The more damage incurred by grain-grain collisions, the less energy is left to pass on and incur motion in neighbor grains. At the same time, amplification of acoustic energy might occur

because grains will radiate more acoustic energy in collisions that result in fracture. Grains that are more prone to fracture may produce more noise than those that are more prone to damage plastically.

Both of these mechanisms likely play a role in the results observed in these experiments. Figure 2 shows that the fluorite experiments dilated more than other samples, which supports damage-dampening of fluctuation energy, however the differences in dilation are more subtle than the differences in acoustic energy which supports amplification of acoustic energy.

Within the range of elastic properties relevant to geologic processes, the implication of damage-dampening of fluctuation energy is that the presence of weak grains in a granular system will impede transmittance of fluctuation energy in a granular flow and contribute to localization of flows, as well as strengthen the composite effect of shear velocity on flow dilation or pressure. In addition, the role of acoustic energy amplification is important for correctly interpreting signals recorded in future field or laboratory experiments and in developing a more complete energy balance for high velocity granular flows.

More generally, it is important to note that this study shows that the rheology of any granular system that is influenced by fluctuation energy will also depend on the material properties and mineralogy of the constituent grains in a predictable way. Such systems are not confined to high velocity shear, as previous work has shown that granular shear flows with low or intermediate shear velocities have measurable responses to internally induced or externally applied fluctuation energy (Siman-Tov,

2018; van der Elst 2012). Such systems are therefore also dependent on the properties of the grains involved in the flow.

It will be important to find what scales of grain angularity and roughness amplify these effects as observed in these experiments, and if there are naturally occurring scales of smoothness and roundness that behave in high velocity shear as predicted by models relying on coefficient of restitution.

Conclusion

Acoustic energy and dilation were measured during high velocity shear at nine steady state velocities between 50 rad/s – 300 rad/s for five mineral sands of differing material properties. We compared how the relationship between dilation and acoustic energy changes with shear velocity across six material properties. The best predictor of $d(\Delta h/\Delta E_a)/dI$ is plastic displacement length, δ. Relative lengths of plastic displacement represent relative amounts of plastic work that accompany grain contact and fracture. In this way δ incorporates elastic modulus, yield strength and fracture toughness.

References

Akono, A.-T., Reis, P. M., & Ulm, F.-J. (2011). Scratching as a Fracture Process: From Butter to Steel. *Physical Review Letters*, *106*(20), 167. http://doi.org/10.1016/S0257-8972(00)01097-5

Andreotti, B., Forterre, Y., & Pouliquen, O. (2013). Granular Media: Between Fluid and Solid. New York: Cambridge Univ Press.

Barenblatt, G. I. (1962). The mathematical theory of equilibrium cracks in brittle fracture. *Adv. Appl. Mech.,* 7, 55.

Broz, M. E., Cook, R. F., & Whitney, D. L. (2006). Microhardness, toughness, and modulus of Mohs scale minerals. *American Mineralogist*, *91*(1), 135–142. http://doi.org/10.2138/am.2006.1844

Campbell, C. S. (2006). Granular material flows – An overview. *Powder Technology*, *162*(3), 208–229. http://doi.org/10.1016/j.powtec.2005.12.008

Glielmo, A., Gunkelmann, N., & Pöschel, T. (2014). Coefficient of restitution of aspherical particles. *Physical Review E*, *90*(5), 052204. http://doi.org/10.1063/1.4811898

Griffith, A. A. (1921). The phenomena of rupture and flow in solids. *Phil. Trans. R. Soc. Lond. A*, 221, 163.

Haff, P. K. (1983). Grain flow as a fluid-mechanical phenomenon. *Journal of Fluid Mechanics*, *134*, 401–430.

Hertz, H. (1896). Miscellaneous Papers (translated by Jones, D.E. and Schott, G.A.), p. 178-180. London: Macmillan and Co., Ltd.

Irwin, G. R. (1958). Fracture. In *Handbuch der Physic.* Springer-Verlag, Berlin, Vol. 6, p. 557.

Jenkins, J. T., & Savage, S. B. (1983). A theory for the rapid flow of identical, smooth, nearly elastic, spherical particles. *Journal of Fluid Mechanics*, *130*, 187–202.

Johnson, K. L. (1985). Contact Mechanics. Cambridge: Cambridge University Press.

Lawn, B. R., & Marshall, D. B. (1979). Hardness, toughness, and brittleness: an indentation analysis. *Journal of the American Ceramic Society*, *62*(7-8), 347–350.

Lawn, B.R., Evans, A.G., and Marshall, D.B. (1980). Elastic/plastic indentation damage in ceramics: the median/radial crack system. *Journal of the American Ceramic Society*, 63, 574-581.

Lawn, B. R. (1993). Fracture of Brittle Solids—Second Edition. Cambridge: Cambridge University Press.

Orowan, E. (1955). Energy criteria of fracture. *Weld. Res. Supp.*, 34, 157-s.

Siman-Tov, S., & Brodsky, E. E. (2018). Gravity-Independent Grain Size Segregation in Experimental Granular Shear Flows as a Mechanism of Layer Formation. *Geophysical Research Letters*, *65*(5), 51,302. http://doi.org/10.1016/0032-5910(76)80053-8

Tabor, D. (1951). The Hardness of Metals. Oxford: Clarendon Press.

Tabor, D. (1970). The hardness of solids. *Review of Physics in Technology*, 1(3), 145-170.

Taylor, S., & Brodsky, E. E. (2017). Granular temperature measured experimentally in a shear flow by acoustic energy. *Physical Review E*, *96*(3). http://doi.org/10.1103/PhysRevE.96.032913

van der Elst, N. J., Brodsky, E. E., Le Bas, P.-Y., & Johnson, P. A. (2012). Auto-acoustic compaction in steady shear flows: Experimental evidence for suppression of shear dilatancy by internal acoustic vibration. *Journal of Geophysical Research*, *117*(B9), B09314. http://doi.org/10.1029/2011JB008897

Young, T. (1845). Course of Lectures on Natural Philosophy and the Mechanical Arts. London: Taylor and Walton.

Appendix A

A.1 Conditioning and Experimental Protocol

Grain size of samples was measured using a Retsch Technology Camsizer Particle Analyser at the University of Pennsylvania, with size distributions shown in Figure A1.1.

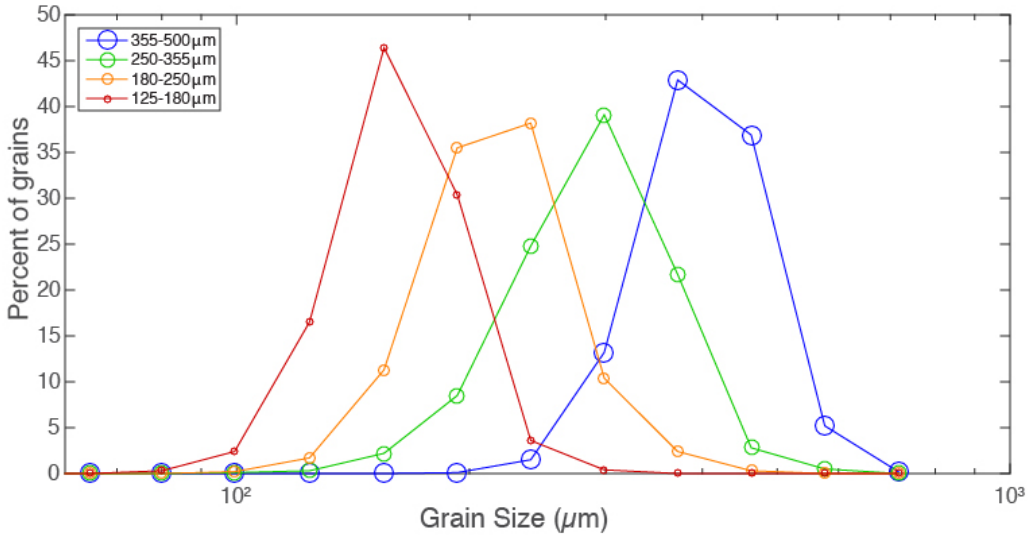

Figure A1.1: Grain size distributions are shown for four size ranges of quartz beach sand from Natural Bridges Beach and Cowells Beach in Santa Cruz, CA. Grain size was measured using a Retsch Technology Camsizer Particle Analyzer.

Each sample was conditioned prior to data collection using the following protocol:

1x	3600s at $1x10^{-3}$ rad/s
1x	650s continuously increasing velocity 25 rad/s – 300 rad/s 650s continuously decreasing velocity 300 rad/s – 25 rad/s
9x	1000s continuously increasing velocity 25 rad/s – 300 rad/s 1000s continuously decreasing velocity 300 rad/s – 25 rad/s

Experimental data shown from the steady state stepped velocity ramps was collected using the following protocol:

3x stepwise increasing velocity from 25 rad/s – 300 rad/s in 12 logarithmically spaced velocity steps, held for 60s each
stepwise decreasing velocity from 300 rad/s – 25 rad/s in 12 logarithmically spaced velocity steps, held for 60s each

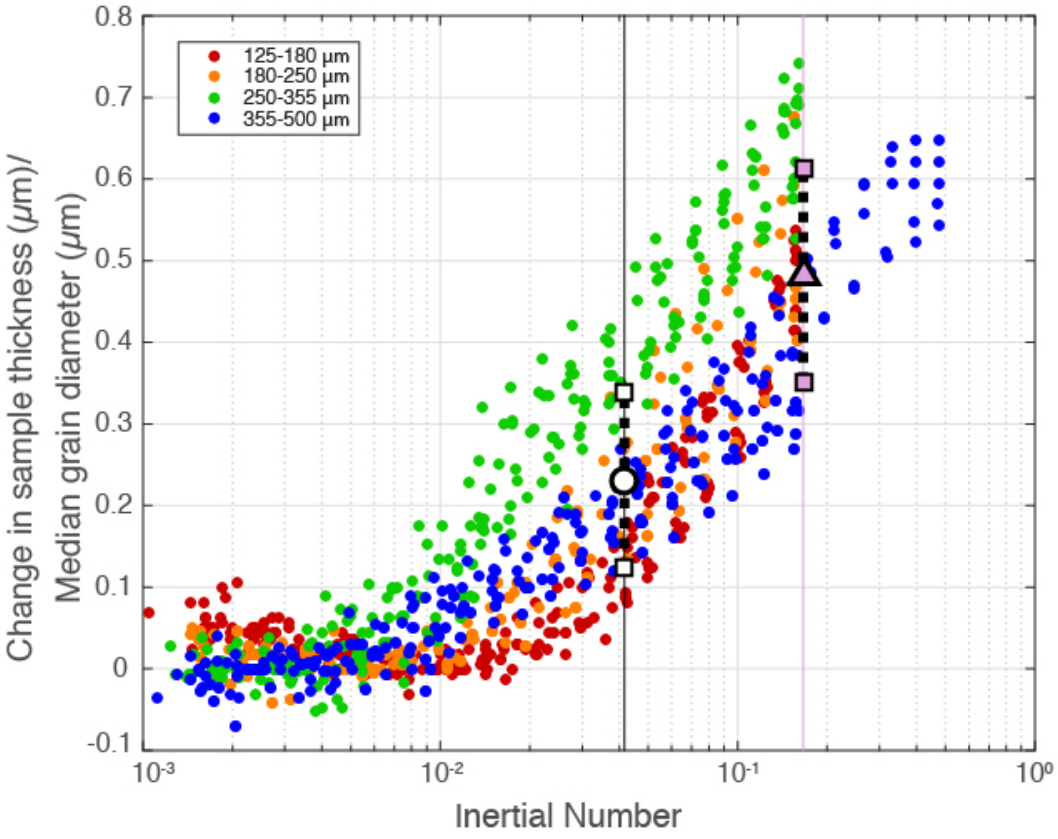

Figure A2.1: Black line shows the lowest inertial number tested in the current investigation. White circle marks the mean dilation above the minimum sample height, as observed in low shear velocity tests plotted here. Purple line shows a different inertial number at which average dilation was calculated to compare effect of reference dilation on fit and error. Purple triangle marks mean dilation above the minimum for this higher inertial number.

A.2 Error Propagation Method

Velocity ramp experiments run at velocities between $I = 10^{-6}$ and $I = 10^{-1}$ showed a minimum sample height achieved between $I = 10^{-3}$ and $I = 10^{-2}$. Figure A2.1 shows change in sample height from the minimum, or critical, height with the solid black line indicating $I = 4.16\text{x}10^{-2}$, the lowest inertial number tested in the higher velocity experiments, i.e. inertial number at 25 rad/s, discussed in the main body of the paper.

The mean dilation of all sizes at shear velocity represented by $I = 4.16\text{x}10^{-2}$ is 0.2309±0.1078 grain diameters. The error in the dilation amount at $I = 4.16\text{x}10^{-2}$ represents the error in our estimation of critical height. For these experiments, the stress is controlled but the volume is not, and each experiment is begun with more sand in the sample cylinder than will ultimately be integrated into the shear zone. Therefore estimating the true minimum shear zone height of the sample could involve using digital imaging techniques to measure the height of the shear zone.

As an alternative, in order to show a measurement of change in sample height from critical height divided by grain diameter, measurements were taken zeroing the sample height to the height at the start of the steady state velocity steps after conditioning steps were complete (see Chapter 1 Figure 3a). The mean dilation determined in Figure A2.1 was added into the mean gap height as measured by the rheometer and zeroed to the start of the three steady state velocity runs. Figure A2.2 shows the progression of the data as error is added in.

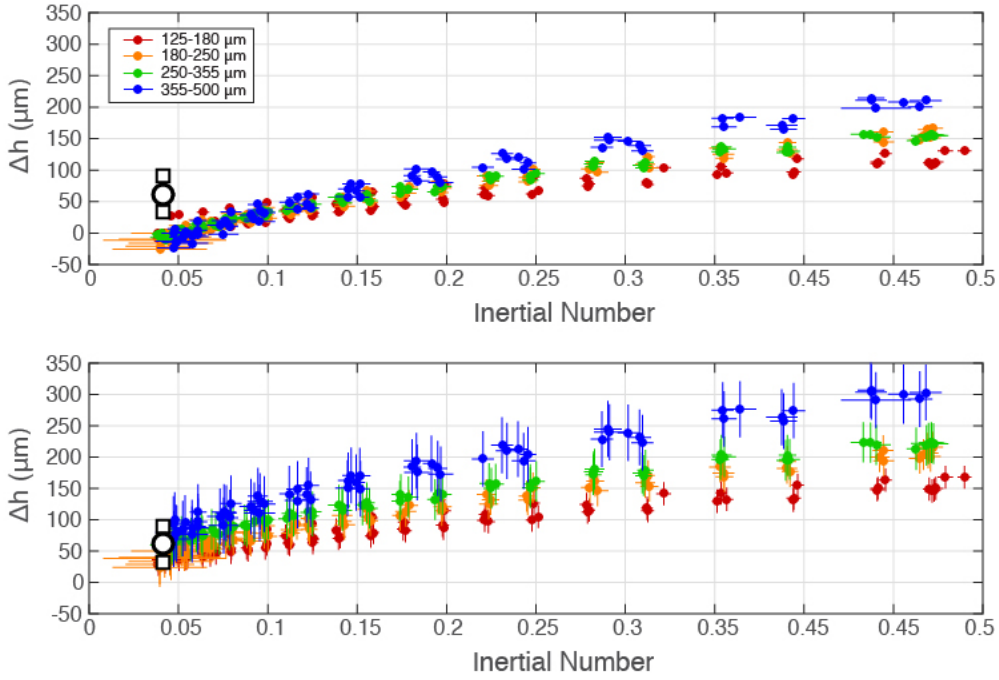

Figure A2.2: Top shows change in sample height from starting velocity. Bottom shows adjusted sample height based on average dilation at this initial velocity (from Fig A2.1).

We tested sensitivity to different reference velocities by using the same procedure to pull out the mean dilation at a higher velocity than that referenced in Figure A2.1. Figure A2.3 shows the effect of zeroing sample height data based on the mean dilation for all grain sizes at an inertial number of $I = 0.16$. The fit relationship between sample height and inertial number is consistent regardless of which reference velocity is used.

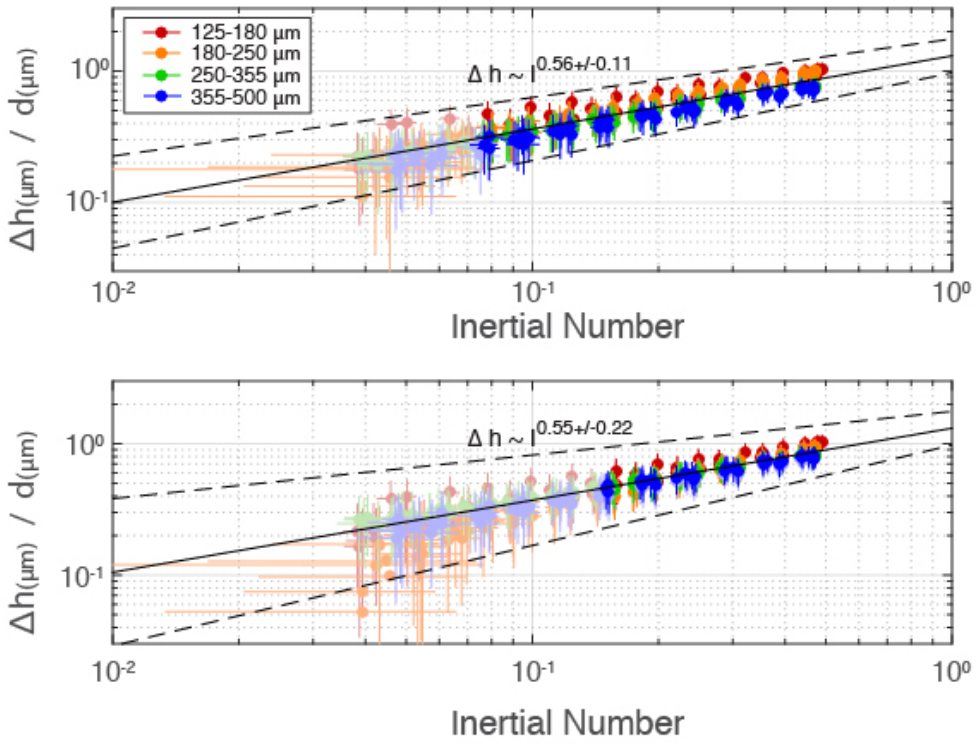

Figure A2.3: Top shows change in sample height with inertial number for data zeroed using dilation at I = 4.16 x 10-2 as reference dilation. Bottom shows change in sample height with inertial number for the same data zeroed using dilation at I = 0.16 as reference dilation. Fit of this data is compatible regardless of reference dilation used.

A.3 Dependence of Acoustic Energy on Grain Mass

The dependence of acoustic energy on grain mass was tested by fitting the function

$$m d^n = \left(\frac{E_a}{I} \right). \tag{A1}$$

If acoustic energy scales with grain mass, then when measured from four grain size ranges of the same composition the acoustic energy should scale with grain volume, or grain diameter cubed. Figure A3.1 shows the fit to equation A1.

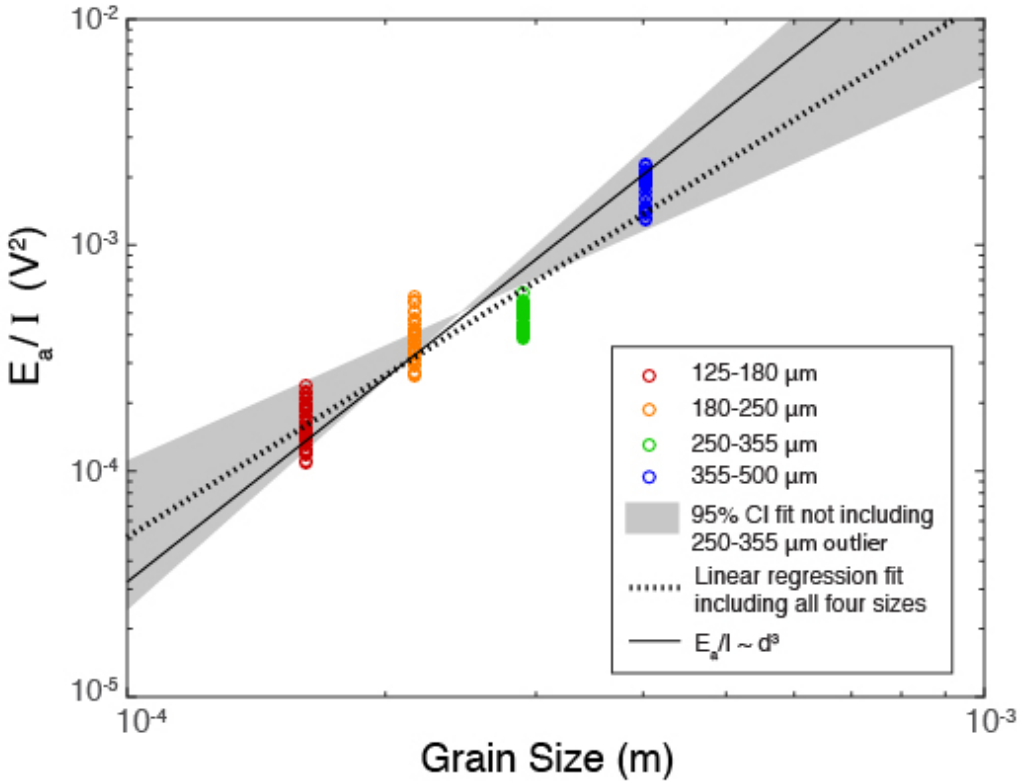

Figure A3.1: Colors correspond to the four grain size ranges tested, plotted at their median grain sizes 162 µm (red), 216 µm (orange), 290 µm (green), and 402 µm (blue). The dashed line shows linear regression fit to all four grain sizes, where n=2.37+/-0.82 (95% CI). Acoustic energy data from the experiment testing 250-355 µm diameter sands (green) were systematically lower than the other three grain sizes tested. The gray shaded region shows the 95% confidence interval for linear regression fit when this outlier grain size is not included in fit. For this fit n=2.54+/-0.84. The solid line shows n=3 for reference.

Figure A3.2 shows a difference in conditioning between some of the grain sizes that may affect this fit. For the 125-180 µm, 180-250 µm and 355-500 µm grain size ranges, conditioning resulted in a decrease in acoustic energy of about 20% from the beginning of the experiment to the final three steady state increasing and decreasing cycles that were used for analysis. For the 250-355 µm grain size, however, acoustic energy decreased almost 40% over the course of conditioning. This

could be due to a circumstantial difference in the sample's reaction to conditioning, or a systemic difference in the position of the accelerometer with respect to the shear band.

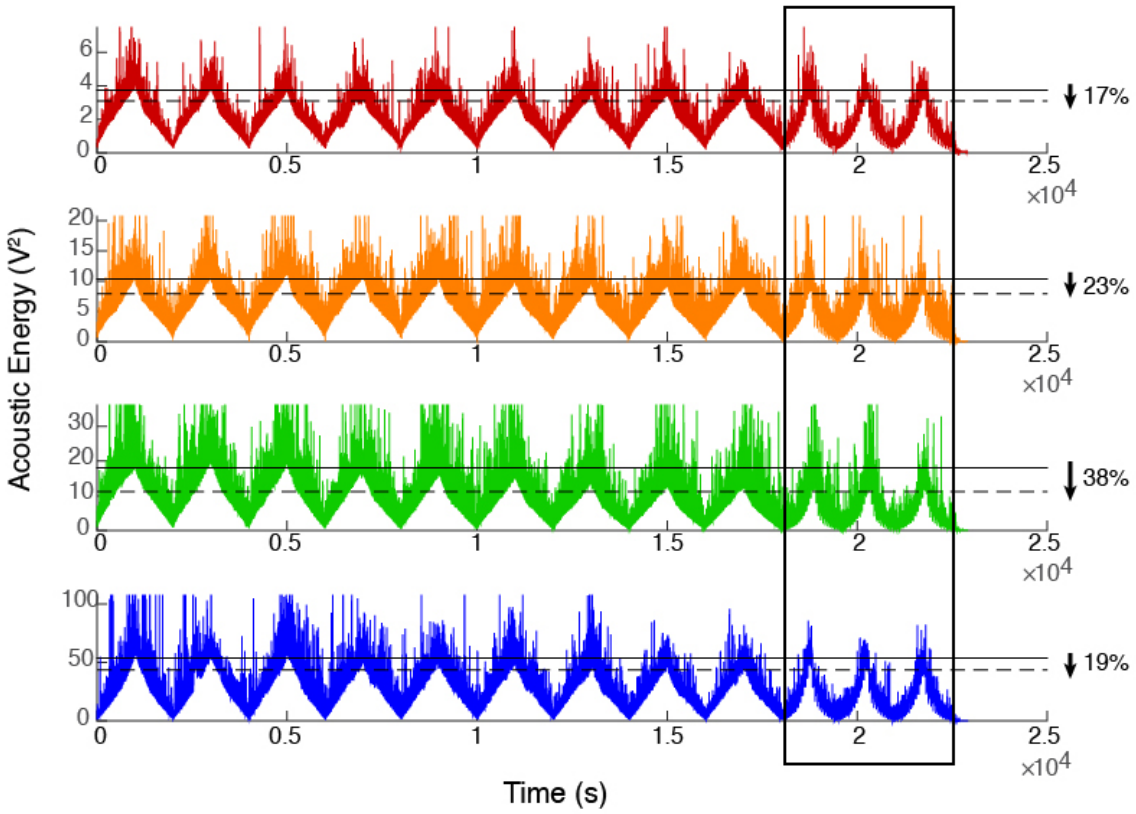

Figure A3.2: All four panels show acoustic energy over the course of conditioning and data collection cycles described in Appendix A Section 1. Top panel shows 125-180 µm grain size (red), second panel shows 180-250 µm (orange), third panel down shows 250-355 µm grain size (green) and bottom panel shows 355-500 µm grain size sample (blue). Solid lines show the average acoustic energy at the lowest threshold of the highest velocity, i.e. the base of the peak noise value recorded during one conditioning cycle, for the first three increasing and decreasing cycles of conditioning. The dashed lines show this threshold value for the final three steady state velocity cycles which is the data used for analysis. For 125-180 µm, 180-250 µm and 355-500 µm grain sizes this threshold dropped an average of 20% over the course of conditioning, but for the 250-355 µm grain size this threshold dropped almost twice as much, 38%.

Because of this difference the 250-355 μm range is not included in the fit to equation S1 shown by the gray shaded region in Figure S3.1, which shows the fit of n=2.54+/-0.84. The scaling with grain diameter cubed, n=3, falls comfortably within this range of fits.

Appendix B

B.1 Experimental details

Vibration Test Experiment

Vibration and acoustic noise perturb the contacts and packing organization of granular materials. This effect has long been observed (Djiksman et al. 2013; Jaeger et al., 1989). To understand the effect of vibration on slowly shearing angular grains, we conduced vibration experiments on four grain sizes of angular quartz sand while under low velocity shear. Samples were sheared in the TA instruments AR2000ex torsional rheometer at 10^{-3} rad/s in a 1 cm radius sample cell, producing edge velocities of 10 μm/s. Samples were subjected to five vibrations in the following order:

2 high amplitude
2 low amplitude
1 high amplitude.

Vibrations resulted in transient reductions in τ/P (both values measured by the rheometer) and compaction. Pre-vibration sample height was nearly or completely recovered when vibration was removed. Figures B1.1-B1.4 show sample height, coefficient of friction and vibration amplitude for the four grain sizes tested.

The change in friction caused by application of vibration is best fitted with an exponential decay function, but for the sake of comparing data collected in this experiment with previous results and drawing conclusions about the result of smaller-scale vibrations, we use a simple power law fit. Figure B1.5 shows the fit of μ/μ_0.

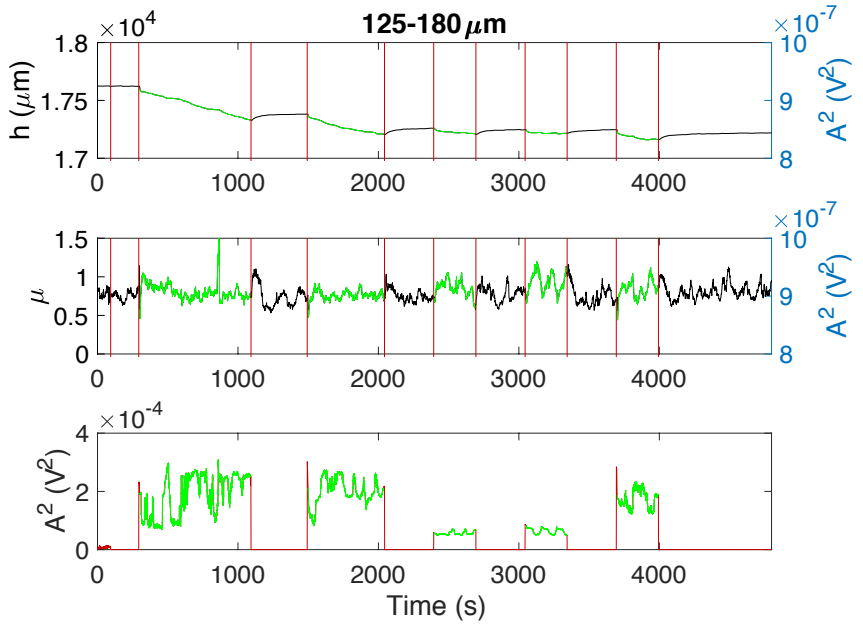

Figure B1.1. Sample height (top), τ/P (center), and vibration amplitude squared (bottom) for vibration test on 125-180 μm diameter angular quartz sand sheared at 10^{-3} rad/s. Green indicates when vibration is on, black indicates when vibration is off, and red lines in top and center plot delineate the start and end of applied vibrations.

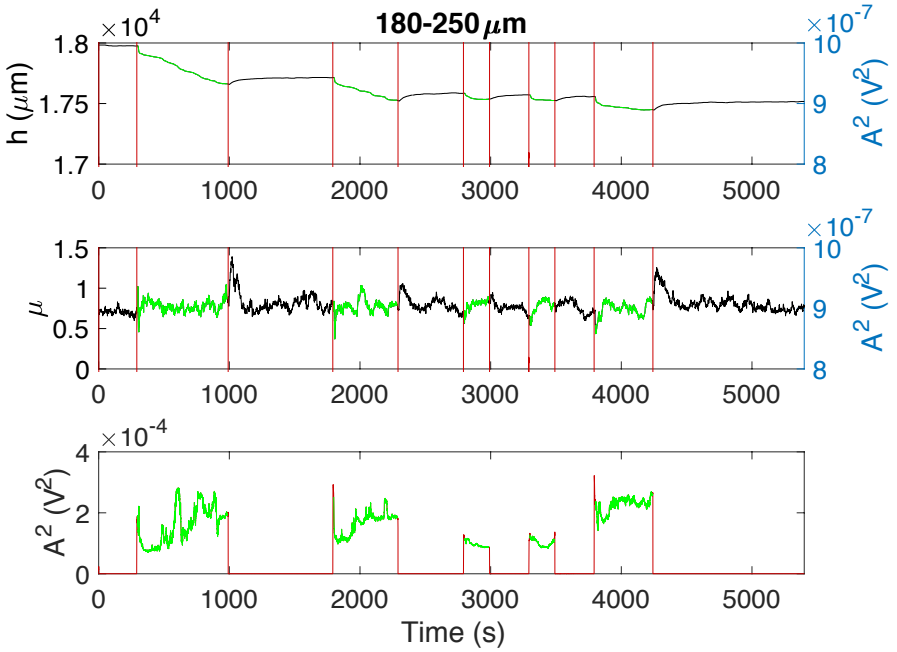

Figure B1.2. Sample height (top), τ/P (center), and vibration amplitude squared (bottom) for vibration test on 180-250 μm diameter angular quartz sand sheared at 10^{-3} rad/s. Green indicates when vibration is on, black indicates when vibration is off, and red lines in top and center plot delineate the start and end of applied vibrations.

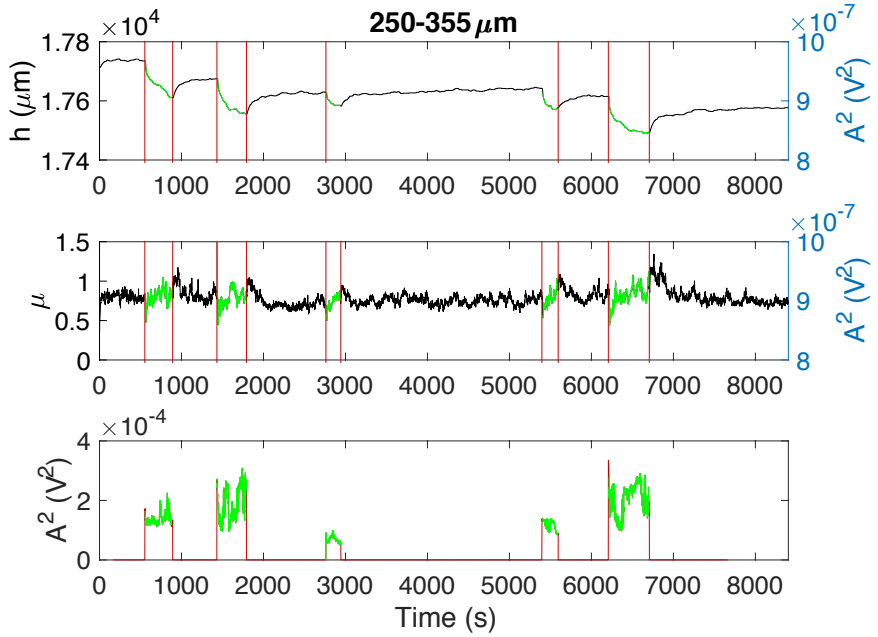

Figure B1.3. Sample height (top), τ/P (center), and vibration amplitude squared (bottom) for vibration test on 250-355 μm diameter angular quartz sand sheared at 10^{-3} rad/s. Green indicates when vibration is on, black indicates when vibration is off, and red lines in top and center plot delineate the start and end of applied vibrations.

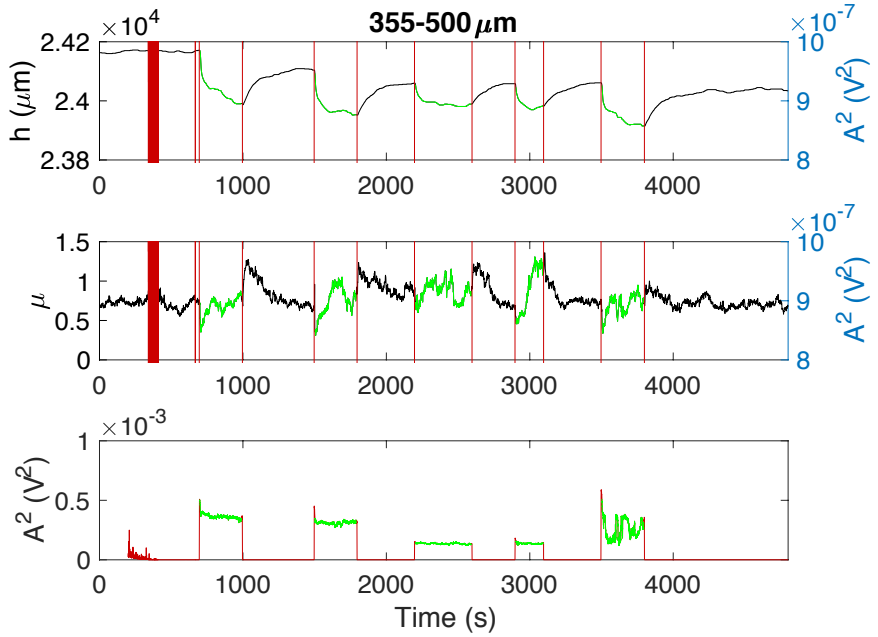

Figure B1.4. Sample height (top), τ/P (center), and vibration amplitude squared (bottom) for vibration test on 355-500 μm diameter angular quartz sand sheared at 10^{-3} rad/s. Green indicates when vibration is on, black indicates when vibration is off, and red lines in top and center plot delineate the start and end of applied vibrations.

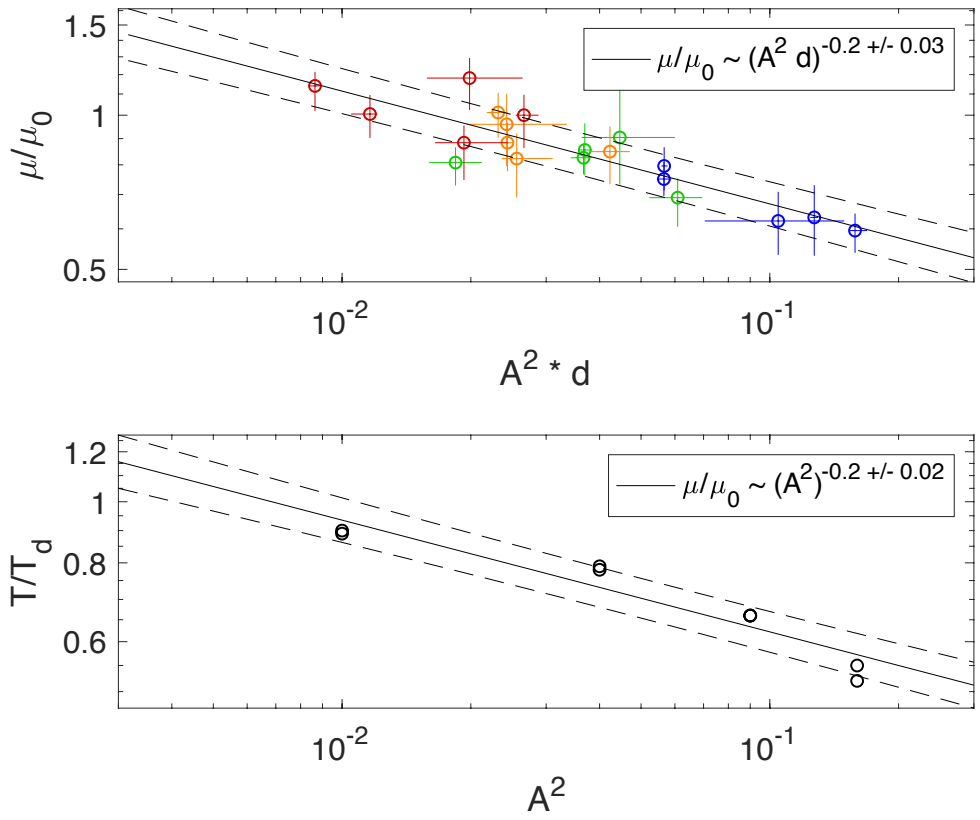

Figure B1.5. (Top) Change in friction for angular quartz grain experiments. Each point represents results from first 30 seconds of vibration for all grain sizes tested. 125-180 μm (red), 180-250 μm (orange), 250-355 μm (green), and 355-500 μm (blue). (Bottom) Change in torque for glass bead experiments conduced for Dijksman et al. 2013. Fit of function for only those T/T_d values in the same range of those tested in the experiments presented here.

The μ/μ_0 compares μ as measured during the first 30 seconds of vibration to μ_0, the average value of μ for the 100 seconds before vibration began. This value is plotted against recorded acoustic amplitude multiplied by grain size in order to account for the difference in attenuation for different grain sizes. Applied vibration will dissipate at each grain contact. To normalize vibration energy, we would therefore wish to divide by number of grains, and over any given length L, the number of grains will be

N=L/d. Therefore $A^2/N \sim A^2d$. When the power law fit of μ/μ_0 with A^2d for the experiments presented here is compared to a power law fit over the same range of μ/μ_0 values measured in the vibration experiment conducted by Dijksman et al. 2013, we find the best fit is with the same exponent: $\mu/\mu_0 \sim (A^2)^{-0.2}$. So we see that at least as far as friction goes, vibration amplitude appears to have a similar effect on the overall coefficient of friction for shear flows made of angular sands or spherical beads. The better function to fit these data with is an exponential decay function, however in the absence of calibrated vibration amplitude values, the power law fit suffices.

We also consider compaction observed during vibration. Figure B1.6 shows compaction as a function of acoustic vibrations. For compaction we normalize acoustic energy based on the mass of the grain, *m*, the number of grains in a chain, *N*, and the size of the gap needed for a grain to drop into, *w*. Since all grains are quartz with the same material density, the mass of the grain can be represented by the diameter cubed, d^3. The number of grains as before can be represented with just grain diameter, d, and the width of the gap needed for a grain to move into the layer below and cause compaction is also d. These combine based on the following formula:

$$\frac{A^2}{mN} w \sim \frac{A^2}{d^3 d^{-1}} d = \frac{A^2}{d} \tag{B1}$$

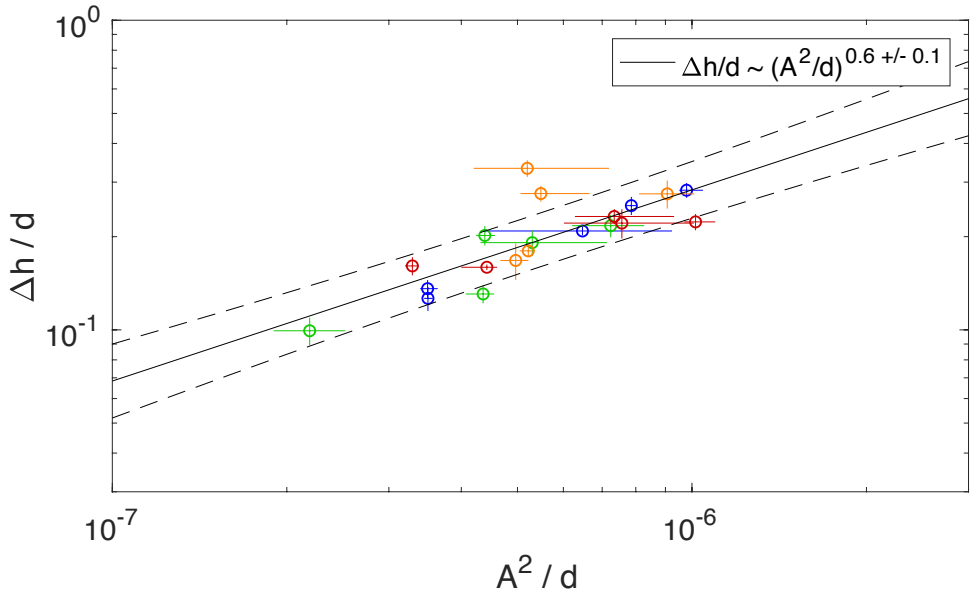

Figure B1.6. Compaction normalized by grain size as a result of applied vibration. Grain sizes include 125-180 μm (red), 180-250 μm (orange), 250-355 μm (green), and 355-500 μm (blue).

Amount of compaction Δh/d represents negative change in sample height after the first 60 s of vibration normalized by grain size. We find that compaction scales with normalized vibration amplitude to a power of approximately 0.6.

Finally, it is observable in the bottom panels of Figures B1.1-B1.4 that for some vibration applications the recorded amplitude wavered. This was due to poor stabilization of the vibration transducer that produced some wobble in the applied vibration. While not intended, this provided us with an opportunity to further test the relationship between vibration, friction and dilation. We cross correlated sample height and friction with acoustic energy data collected while vibration was on. In other words we cross correlated the green portions of the time series shown in Figures

B1.1-B1.4. Figure B1.7 shows cross correlation coefficient functions for friction and sample height and for friction and acoustic energy.

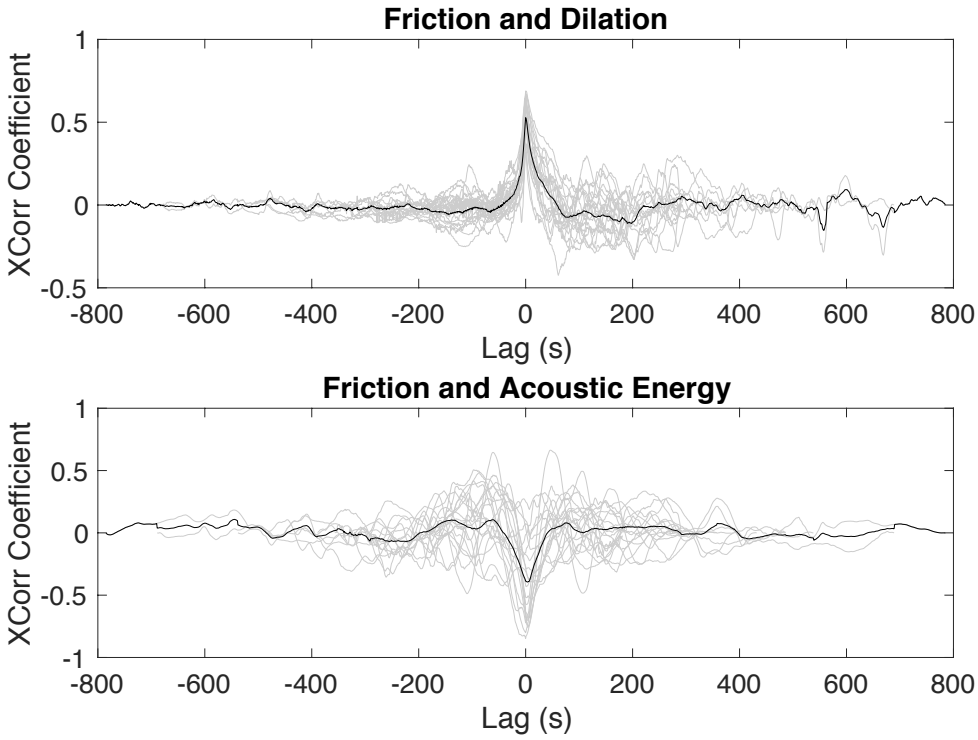

Figure B1.7. (Top) Black line shows average cross-correlation coefficient for friction and sample height during vibration applications. Gray lines show cross-correlation coefficients for each vibration application. (Bottom) Black line shows average cross-correlation coefficient for friction and vibration energy during vibration applications. Gray lines show cross-correlation coefficients for each vibration applications.

The positive cross correlation coefficient between friction and dilation shows that an increase in friction correlates with an increase in sample height, and a decrease in friction correlates with compaction of the sample. There is a slight positive-leaning skew in the cross-correlation coefficient which in this case may imply that the change in friction occurs first and the change in sample height follows. The negative cross correlation coefficient between friction and acoustic energy from

vibration shows that an increase in acoustic energy is correlated with a decrease in friction, as we have observed through other analysis. It is interesting that even transiently and due to small-scale oscillations, this relationship still holds.

These experiments show that vibrational energy causes reduction in friction and weakening of low velocity granular shear flow. Therefore it is possible that the rheology of grains moving at low velocity *within* a fast moving shear flow would be susceptible to the same vibrationally induced effects as a result of the increase in fluctuation energy produced by the grain collisions that dominate faster moving shear flows.

High Velocity Shear Experiment

Each sample was conditioned prior to data collection using the following protocol:

1x	3600s at $1x10^{-3}$ rad/s
1x	650s continuously increasing velocity 25 rad/s – 300 rad/s 650s continuously decreasing velocity 300 rad/s – 25 rad/s
9x	1000s continuously increasing velocity 25 rad/s – 300 rad/s 1000s continuously decreasing velocity 300 rad/s – 25 rad/s

In order to measure the granular samples as close to steady state as possible at a given velocity, conditioning of the sample was required to minimize the contribution of long term settling of the sample as it shears. Figure 3a and 4a show changes in sample height and acoustic energy, respectively, throughout the conditioning cycles.

Data used for analysis from the steady state stepped velocity ramps was collected after conditioning was complete using the following protocol:

3x	stepwise increasing velocity from 25 rad/s – 300 rad/s and decreasing velocity from 300 rad/s – 25 rad/s in 18 logarithmically spaced velocity steps, held for 60s each

B.2 Composite flow behavior and lowering of base of shear by entrainment

Video images show that grains that are stationary and below the base of shear at the lower velocities tested, are mobilized as the top velocity increases. Therefore this is not a case of the base of flow lowering with increasing driving velocity as a result of compaction of immobilized or barely mobilized grains below the shear zone. If that were the case we would observe these more slowly moving grains moving downward and upward with changes in top velocity. Rather the observation is fully stationary grains at lower velocities are then picked up into the shear flow at higher velocities.

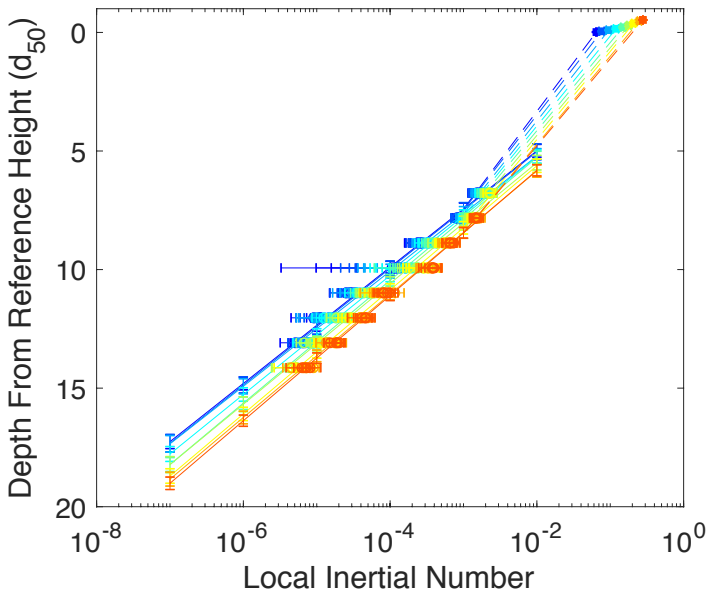

Figure B2.1. Open circles show local inertial number at depth below reference height for nine steady state velocities tested. Solid squares show driving inertial number at top of flow. Solid lines show velocity profiles based on particle image velocimetry (PIV) analysis. Dashed lines show inferred velocity profiles above PIV detectable velocities. Warmer colors correspond to faster driving velocities and cooler colors correspond to lower driving velocities. As driving velocity increases, top of the flow raises and bottom of flow simultaneously lowers.

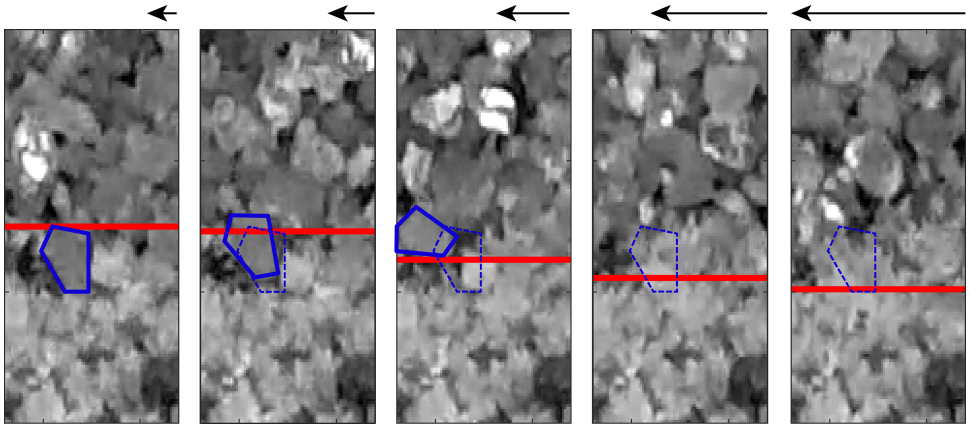

Figure B2.2. Bottom of flow lowers as a result of entrainment of grains with increasing driving velocity. Arrows at top of figure indicates relative driving velocity for each image. Thick red lines show base of flow where local inertial number is 10-6, the lowest detectable velocity using PIV. Thick blue outline shows the location of one easily visible grain for each of several velocities tested, with the relative driving velocity corresponding to each image represented by the length of the arrow above each image. Thin dotted blue outline shows the location of this grain in its original location at the slowest velocity in the series. The grain only moves location as the base of flow dips below the top of the grain outline, and this corresponds with the grain being rolled upward and then in the direction of flow.

Appendix C

Fluorite is the softest mineral tested for these experiments and shows different breakage behavior. While the quartz grains show some breakage of very small pieces in the 10-20 micron size range, fluorite showed a propensity to break into larger pieces, in the 20-80 micron size range. These pieces made up a larger proportion of the volume of the flow, but as Figure S1 shows, volumetrically this did not have a large effect on the distribution of grain sizes in the sample.

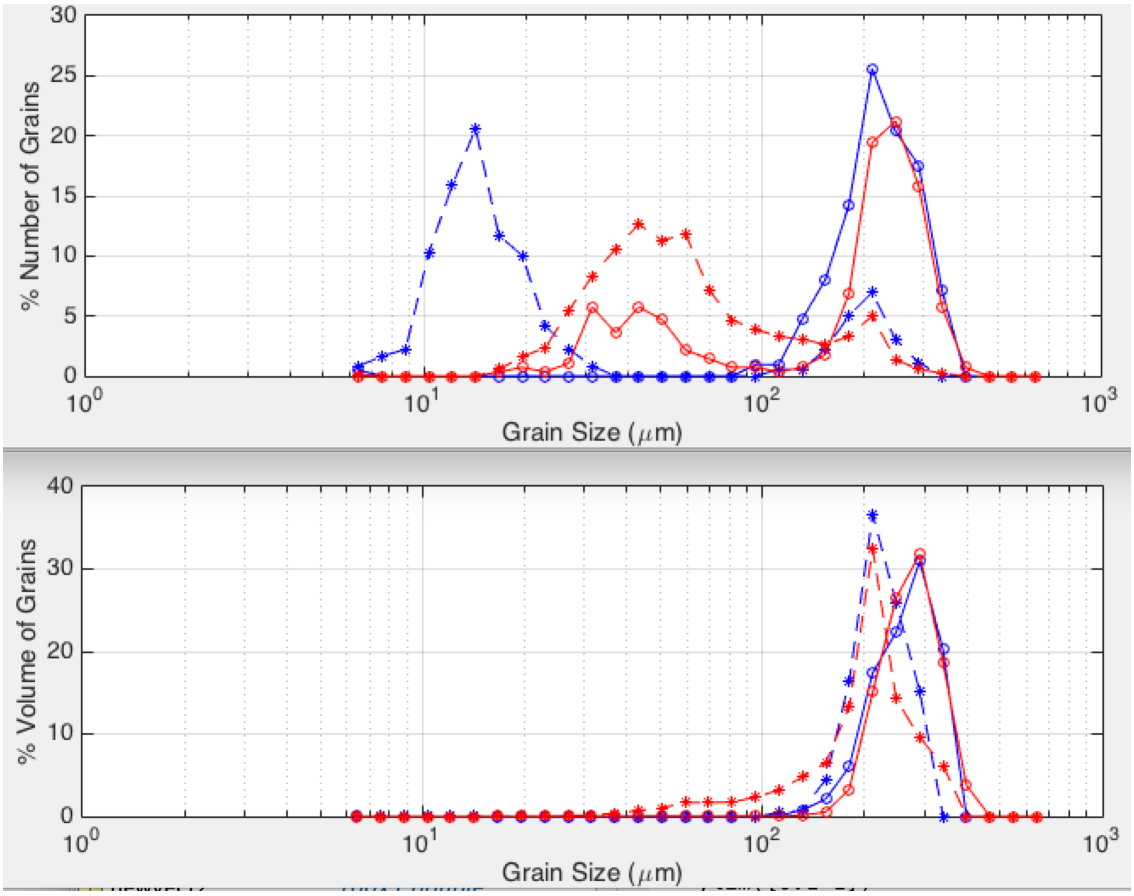

Figure C1.1. Grain size distributions for quartz (blue) and fluorite (red) by number of grains (top) and by volume (bottom). Open circles are size distributions before shear and stars are size distributions after shear.